DISSERTAÇÃO

Neoclassical Transport of Particles in Magnetic Confined Plasmas

Felipe Nathan de Oliveira Lopes

Brasília, Março de 2017

UNIVERSIDADE DE BRASÍLIA

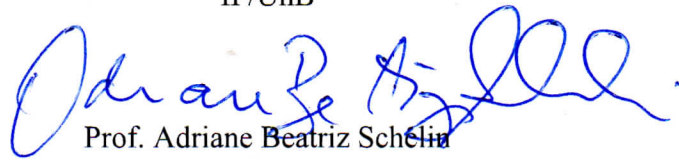# "Neoclassical Transport of Particles in Magnetic Confined Plasmas."

Por

Felipe Nathan de Oliveira Lopes.

Dissertação submetida ao Instituto de Física da Universidade de Brasília como parte dos requisitos para a obtenção do grau de Mestre em Física.
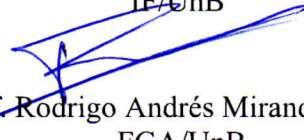
Aprovada por:

Prof. Ivan Soares Ferreira
IF/UnB

Prof. Adriane Beatriz Schelin
IF/UnB

Prof. Rodrigo Andrés Miranda Cerda
FGA/UnB

Prof. Dr. Fernando de Oliveira Albuquerque
Coordenador de Pós-Graduação
Instituto de Física

FICHA CATALOGRÁFICA

REFERÊNCIA BIBLIOGRÁFICA

LOPES, F. (2017). *Neoclassical Transport of Particles in Magnetic Confined Plasmas.* Dissertação, Instituto de Física, Universidade de Brasília, Brasília, DF, 78 p.

CESSÃO DE DIREITOS

_____

Felipe Nathan de Oliveira Lopes

Instituto de Física - IFD

Universidade de Brasília (UnB)

Campus Darcy Ribeiro

CEP 70919-970 - Brasília - DF - Brasil

Agradecimentos

Eu gostaria de dedicar este trabalho, primeiramente, ao meu professor e orientador, Ivan Ferreira, que mesmo nesta situação peculiar com a qual eu me encontro, continuou com o trabalho apesar do esforço extra, e que no decorrer da minha graduação me ensinou coisas nao somente relacionadas ao conteúdo acadêmico mas também, e tão importante quanto, da vida.

Eu dedico também aos meus pais, Katia Aparecida e Gilson de Oliveira, e meu irmão, Yuri de Oliveira, que estiveram sempre do meu lado nos momentos em que nada fazia sentido para mim, e ainda continuam, porque as coisas ainda não fazem tanto sentido quanto eu acredito que deveriam fazer, por todo o carinho e atenção que eles me deram eu serei eternamente grato. Dedico à minha esposa, Estel Villaronga, que entrou na minha vida de uma maneira particular e tem sempre me apoiado, e que, por algum motivo, enxerga o sentido das coisas que eu nao sou capaz de enxergar. Dedico à todos os meus amigos, da minha cidade natal, Gama, onde eu cresci e aprendi o conceito de amizade, especialmente ao Caio e ao "bonde do Voyagem".

Dedico também aos meus amigos e companheiros da Universidade de Brasilia, aos que se foram, e aos que ainda estao por aqui, eles fazem definitivamente parte de uma importante e inesquecível etapa da minha vida. Lucas, Lilah, Rodrigo, Patricia, Artur, Suzane, Piri, e a muitos outros. Um agradecimento especial também à Coordenação de Aperfeicoamento de Pessoal de Nível Superior, CAPES, pelo apoio financeiro e pelo seu trabalho no fomento à pesquisa de pós-graduação stricto sensu no Brasil.

Felipe Nathan de Oliveira Lopes

RESUMO

Plasmas confinados em diferentes topologias magnéticas são uma tarefa importante na busca pela Energia de Fusão. Hoje em dia, as formas mais estudadas de Fusão Termonuclear Controlada focam em Confinamento Inercial, Stellarators e Tokamaks. No presente trabalho, estudaremos os diferentes mecanismos de transporte presentes nos plasmas toroidalmente confinados. Vamos rever a teoria a partir dos conceitos básicos de transporte de plasma, até as peculiaridades presentes em plasmas toroidalmente confinados, conhecido como tokamak. Na fronteira do modelo de transporte mais realista, a questão do transporte anômalo será tratada com a teoria do transporte turbulento, no âmbito da teoria girocinética. O uso de ferramentas computacionais auxiliará na análise do impacto das microinstabilidades no fluxo de partículas e calor, e auxiliará na validação dessa abordagem, feita com uma análise da literatura.

ABSTRACT

Plasmas confined in several magnetics topologies are an important task in the quest for Fusion Energy. Nowadays, the most studied forms of Controlled Thermonuclear Fusion focus on Inertial Confinement, Stellarators and Tokamaks. In the present work, we are going to study the different transport mechanisms present in toroidally confined plasmas. We are going to review the theory from the basic concepts of plasma transport, until the peculiarities present in toroidally confined plasmas, known as tokamak. In the border of the realistic transport model, the issue of the anomalous transport will be treated with the turbulent transport theory, in the framework of the gyrokinetic theory. The use of computational tools will help us to assist the analysis of microinstabilities impact on flux levels, and to give support in the validation of this approach, done with a thorough analysis the literatures.

TABLE OF CONTENTS

LIST OF FIGURES

LIST OF TABLES

LIST OF SYMBOLS

Latin Symbols

Q	Heat Flux
V_ζ	Toroidal Flow Velocity
$\hbar$	Planck's Constant

Greek Symbols

Γ	Particle Flux
χ_i	Heat Diffusivity
σ	Electrical conductivity
Ψ	Flux Surface
ν	collisional frequency
μ	Magnetic Momentum
Π	Viscous Stress
γ	Instability Growth Rate
ω	Instability Frequency

Dimensionless Constants

e	Euler Constant
π	pi Constant
i	Imaginary Number

Acronym

ITER	International Tokamak Experimental Reactor
JET	Joint European Torus
ITG	Ion Temperature Gradient
ETG	Electron temperature Gradient
TEM	Trapped Electron Mode
ITB	Internal Transport Barrier
ETB	Edge Transport Barrier

1 INTRODUCTION

1.1 INTRODUCTION

The increasing global energetic consume is reaching limits intolerable for the old means of power production to provide sustainable electric energy. One of the most promising candidate to deal with this issue is the Thermonuclear Controlled Fusion. The aim of this dissertation is to provide an insightful understanding of the transport phenomena in Thermonuclear Plasmas, most precisely anomalous and turbulent transport.

Transport is the study of the mechanism in which mass, energy and momentum are exchanged in a given system. In complex systems such as magnetically confined plasmas, non intuitive effects may appear due to the complexity of the interaction of the different particles with the background field and from the field with the particles. Disregarding the already known non orthodox effects of transport phenomena in magnetized plasmas, new mechanisms that does not fit in the old measurements are treated. Anomalous transport can be considered as the set of divergence of orders of magnitude between neoclassical prediction and real measurements. It is mostly caused by turbulence motion steered by micro-instabilities.

The structure of this monograph is as follows. Chapter 1 discusses a brief introduction to the topic. Chapter 2 presents the mechanism of plasma confinement from the most basic approach, up to the classical model. Chapter 3 discuss more realistic approach to the transport description, and chapter 4 introduces the gyrokinetic solution to the anomalous issue. Chapter 5 introduces and explains the numerical approach, and chapter 6 deals with examples, concluding with chapter 7.

1.2 THE QUEST FOR ENERGY

The world has been passing through important changes since the advent of the late modern era, where the second industrial revolution in the beginning of the 20th century brought the increasing need for new forms of energy in order to nurture a society increasingly dependent on new technologies. In the end of the 19th century, based on the three-phase high-voltage electrical power distribution from Nicolas Tesla, electric grids started to be formed as a main source of distributed and accessible electricity (John W. Klooster, 2009). The uncontrolled onset of the new demand brought together an inconvenience. Global temperature increase was reported by different agencies in different countries world wide. Alternative forms of fuel, contrary to the ordinary coal and gas, were needed but not noticed until the mid 20th century. Beyond the large

impact on global warming, the rate of increase in consumption and population growth represent a real treat to a sustainable evolution.

To discontinue technological progress is unfeasible and unreasonable. A new strategy in the approach to progress needs to be taken. A brighter future is foreseen only if together with an improvement of the status quo of the environmental panorama. Innovative energy sources are needed and more efficient energy storage mechanism needs to be developed, in order to minimize the effects caused by the enormous amount of gases released in the atmosphere during the last century and to mitigate any other effect that may have impact in the environment whatsoever.

1.3 NUCLEAR ENERGY

In 1932, Ernest Rutherford was reported to have discovered that lithium atoms, when split by protons, could release energy, in agreement with the mass-energy equivalence principle established by Albert Einstein (Richard Rhodes, 1986). The late discovery of the neutron by James Chadwick opened a path to what is known as the atomic era, where the nuclear energy was used as an alternative form of electric energy and as a novel weaponry mechanism.

Nuclear energy is considered as all the energy that is provided by the break down or fusion of nuclear particles (John R. Lamarsh, 2001). Two approaches are known, the one involving the breakdown of heavy atom, known as Nuclear Fission and another one associated with the fusion of light nuclei, known as Nuclear Fusion.

1.3.1 Nuclear Fission

Nuclear Fission is a subatomic process in which a heavy nucleus undergo a decay to another nuclei with lighter atomic mass and is followed by the release of an amount of energy correspondent to the difference in the biding energies of the primary nucleus and the two remaining nuclei. It is important to understand that a Nuclear Reaction is caused by neutron bombing the heavy and unstable nucleus, also know as radioactive decay, described as a spontaneous break of the nucleus due to quantum mechanics effects acting within the subatomic particles. An example of Nuclear Reaction, followed by the nucleus split and energy release is described as follows

$$\,^{1}_{0}\text{n} + \,^{235}_{92}\text{U} \rightarrow \,^{141}_{92}\text{Ba} + \,^{92}_{36}\text{Kr} + 3\,^{1}_{0}\text{n} + Energy \tag{1.1}$$
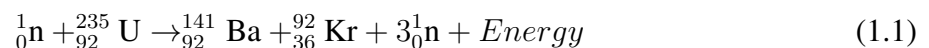
A neutron collides with the nucleus of $^{235}_{92}$U and as a result the nucleus is split in two lighter elements and three new neutrons. The amount of energy released in this reaction is approximately $200 MeV$.

The issue with the Nuclear Fission processes is the reaction chain. The three neutrons released in the reaction 1.1 collide with three new nuclei and give rise to a chain of reaction that increases its energy release exponentially. Controlled Nuclear Fission is a deep and complex field of study that requires deep knowledge of the interplay of nuclear forces and feedback mechanism to the proper management of the chain reaction. Another important issue with Nuclear Fission is the radioactive waste. Since the products of the Nuclear Reactions are in its majority radioactive, the process generates enormous amounts of material radioactively contaminated, and in cases of human negligence or unpreparedness, leaks of contaminated material to the environment are cause of concern and fear.

1.3.2 Nuclear Fusion

Contrary to the Nuclear Fission, Nuclear Fusion is a process in which two light nuclei, in general Hydrogen isotopes, are put together and combine, originating a heavier element, generally helium. Nuclear Fusion is the main form of energy release in all the stars in the Universe and the pursuit of this form of energy on earth has been driving a considerable effort from humankind. In order to maximize the effective cross section, the most effective elements used are the Deuterium, $^2_1$H, and the Tritium, $^3_1$H. The reaction is described as follows

$$^2_1\text{H} + ^3_1\text{H} \rightarrow ^4_2\text{He} + ^1_0\text{n} + Energy \tag{1.2}$$

In the case of heavenly bodies like stars, it is important to notice that the main chain of fusion reaction of such bodies with the mass of the sun or less, is the proton-proton chain reaction.

$$^1_1\text{H} + ^1_1\text{H} \rightarrow ^2_2\text{He} + \gamma \rightarrow ^2_1\text{H} + \text{e}^+ + \nu_e + 0.42 MeV \tag{1.3}$$
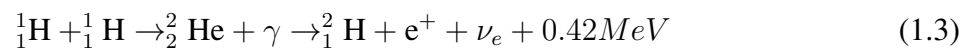
It is necessary to remember also that, due to the high value of mass, the gravitational pressure of the sun exert enough force to keep the plasma confined, and high values of kinetic energy are possible to be achieved by the protons due to the counterbalancing of the gravitational effect. In the case of earthly magnetic confinement, the most common approach is using magnetic fields, and as an alternative, a reaction with Deuterium Tritium is chosen due to its high cross section and higher values of energy released.

Figure 1.1 shows us the different nature of the biding energy for different atomic numbers. It is seen that the energy released per nucleon in the case of fusion reactions is larger than the energy released in the fission case.

The temperatures necessary to Nuclear Fusion reactions to occur in a laboratory are of the order of tens of KeV, contrary to the hundreds of KeV expected to overcome the Columb barrier
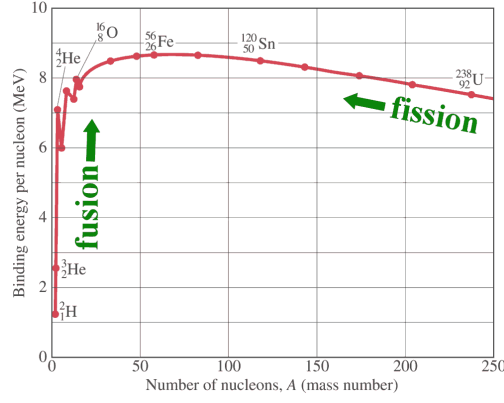
Figura 1.1: Biding energy for different isotopes [reference:Pearson Prentice Hall]

of the two charged particles (Shultis, J.K. 2002), this is possible due to a mechanism known as the Quantum Tunneling.

In Quantum Mechanics, particles are described as wave functions and their temporal behavior is implied from the Schrödinger wave equation. In this scenario, the particle's observables is extracted as the result of a probability density function.

$$i\hbar\frac{\partial\Psi(\mathbf{r},t)}{\partial t} = \left[\frac{\hbar^2}{2\mu}\bigtriangledown^2 + V(\mathbf{r},t)\right]\Psi(\mathbf{r},t) \tag{1.4}$$

Schrödinger equation (1.4) describes the time evolution of the quantum state of a system, where $\Psi(\mathbf{r},t)$ is the wave function, and $V(\mathbf{r},t)$ represents the potential in which the particle is submitted. By means of Fourier analysis, Equation 1.4 can be solved and the resulting equation 1.5 is the wave-like direct solution of Schrödinger equation, validating a non corpuscular interpretation.

$$\Psi(\mathbf{r},t) = \frac{1}{(\sqrt{2\pi})^3}\int \Phi(k)e^{i(\mathbf{k}\cdot\mathbf{r}-wt)}d^3\mathbf{k} \tag{1.5}$$

As a consequence of the mathematical formulation, particles are expected to interact in a probabilistic way with potential wells, and due to this mechanism, there is a non zero probability that when faced with a higher potential compared to its own energy, a particle may overcome it. This effect is known as Quantum Tunneling.

In the sun, in order to overcome the Columb repulsion potential, the energy required by the protons would be in the order of thousands of KeV, but due to the Quantum Tunneling effect and the high density in the core, the proton-proton chain reaction takes place more often than classically expected. In laboratory, the same principle is applied.

4

From the reaction 1.2, $17.58 MeV$ is released as energy. The essential point of the Nuclear Fusion is that Deuterium is found in sea water, in the form of heavy water, and the Tritium can be easily bred, making therefore the reaction cheaper and more abundant. In order to fuse, the nuclei must be put close enough to overcome the electrostatic Columb potential. This means a certain amount of energy must be deposited on the system in order to achieve what is known as ignition. Ignition the point where the heat from the fusion reactions is enough to maintain the reaction ongoing without external input and considering all the possible losses. The field of Physics concerned with the study of such reactions is called Plasma Physics.

Plasma Physics is the field of physics concerned with the study of matter when electrons are detached from atoms and behave freely from it.

Due ti the high temperatures required and the complex non linear dynamics of the Plasma, this alternative as an energy source is seen almost as an utopia, but if there is something that humankind learn through the centuries is that a dream dreamt together becomes reality. Due to the absence of uncontrolled chain of reactions and almost no radioactive waste, Nuclear Fusion has an enormous advantage when compared to Nuclear Fission.

1.4 THERMONUCLEAR CONTROLLED FUSION

Thermonuclear Fusion is considered the way to achieve nuclear fusion by means of extremely high temperatures, in order to fulfill the Lawson Criteria. The Lawson Criteria measures a relation between the plasma electron density n_e and the energy confinement time τ_E and gives condition for a fusion reaction to reach ignition. More precisely, the Lawson criteria is a not-so-rigorous principle, as described by J. D. Lawson himself, utilized to envisage the range of values of density and energy confinement time of a burning plasma in order to achieve a self sustained reaction. The equation represents a power balance in thermonuclear reactors in order to get an approximation of the referred quantity.

In the case of the Deuterium-Tritium reaction, for temperatures of the order of $T = 14 keV$, the Triplet Product (J. D. Lawson, 1957) can be approximated by the following relation

$$nT\tau_E \geq 3 \cdot 10^{21} KeV s/m^3 \tag{1.6}$$

Here, n is the density, T is the temperature and τ_E is the confinement time. It can be viewed from the image below that the Lawson criteria can be used as a guide to understand at what values of temperature the product of density n_e and the energy confinement time τ_E are better expected to give rise to a self sustained reaction.
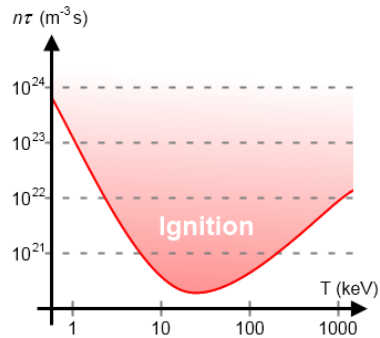
Figura 1.2: Lawson curve for the D-T reaction [reference:Stanford]

Contemplating the above restrictions, some concern must be addressed to the approach in which way the Plasma will be confined, and for how long its facing components will cope with hundreds of million degrees and, furthermore, the best way the avoid instabilities.

In this scenario, two main approaches are considered, Inertial Confinement Fusion (ICF) and the Magnetic Confinement Fusion (MCF). For ICF, lasers may be used in order to compress a pellet of Deuterium-Tritium and induce the fusion process, the system is confined by the inertia of the pallet due to the isotropic alignment of the lasers injection. MCF relays in Electromagnetic heating, together with Neutral Beam Injection, in order to heat up the gas, and a magnetic field in order to confine it. This topic will be further discussed with greater depth.

2 PLASMA CONFINEMENT

The study of toroidally confined Plasmas cannot be accurately performed without a deep understanding of Magnetized Plasma. The need for it comes from the fact that, typical plasma temperature in a fusion device are of the order of, $10 KeV$, as expected in ITER. In such scenario, no known material is capable of coping with such temperatures and therefore, a broad expertise in magnetically confined plasmas is required in order to avoid the melting of plasma facing components.

Whilst dealing with magnetized plasma, a focus in fully ionized matter is required in order to maintain the relevance in regard to core fusion devices. The plasma consist of unbounded ions and electrons, forming a *quasi-neutral* fluid, which means that in a macroscopic first order approximation, the plasma can be considered neutral. When closely analyzed, a parameter known as Debye length plays an important role in defining first and further orders of approximation for of plasma neutrality analysis. The Debye length is a measure of the persistence of electrostatic effects in the plasma, in practical terms, it gives us the scale in which the *quasi-neutrality* can be considered valid. The fact that the plasma does not allow macroscopic charge separation does not mean that there are no electrostatic fields present, in most of the cases a property known as self-organization, vastly present in magnetized fusion plasma, allows the appearance of structures carrying significantly high values of electric fields (M. Mavridis, 2014).

2.1 CONFINEMENT MODELS

Within the MCF approach, different devices designs are often used. Magnetic mirrors pursue the confinement by means of the mirror effect of magnetic fields and the formation of magnetic bottles, structures formed when two diverging magnetic fields are put together. The pinch effect is described as a compression of a filament of current by means of magnetic forces. In this concept, two main devices are studied, the θ and Z pinch machines. In the Z pinch machine, figure 2.1, the current, (yellow), flows in the axis direction, and the magnetic field points to the poloidal direction. Meanwhile in the θ pinch, figure 2.2, the magnetic field, (purple arrow), is the one to stream in the axial direction, whereas the current points to the poloidal direction.

The main problem with the MCF approach described above is the edge physics, *i. e.*, how the plasma can be contained in the beginning and end of the device. In order to solve this problem, a configuration in which the circular ends of the cylinder is joining together was proposed as a solution.
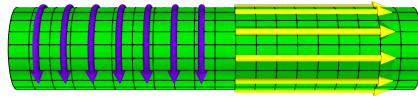
Figura 2.1: Z pinch. Yellow represents the current direction, and purple the magnetic field [credit: DaveBurke].
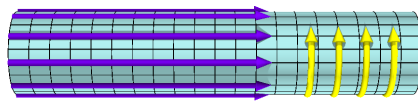
Figura 2.2: θ pinch. Purple represents the current direction, and yellow the magnetic field [credit: DaveBurke].

In topology theory, a Torus, figure 2.3, is a three dimensional solid obtained by the revolving of a circle around a co-planar axis. When used to mold the shape of the plasma where the nuclear fusion reactions are taking place, the torus shape presents the advantage of allowing the magnetic field to have, also, a toroidal geometry. Following the Poincaré–Hopf theorem of differential topology and the Hairy Ball theorem of algebraic topology and its implications in topological properties of n-dimensional folds, the torus is a solid which possesses an Euler characteristic number equal to zero (Jean-Paul Brasselet, 2009), which means we can drawn a continuous vector field in its surface with non vanishing points. It is important to fulfill this criteria because the magnetic field formed in this shape cannot have any vanishing point, since it would lead the plasma to be dislodged from its stability.

Following this geometry, two main models were suggested. The Stellarator, first proposed by Lyman Spitzer in 1950, is a toroidal device in which the non azimuth symmetric magnetic field is twisted in order to avoid drift losses to the containment. When toroidally confined, one of the problems that occurs with the plasma dynamic is that, due to the change in the magnetic field intensity inside and outside of the torus, a magnetic field gradient is generated. The plasma then tends to drift in a direction perpendicular to the magnetic axis and the centrifugal direction, and the reaction is terminated due to plasma losses. When compared to other approaches, the Stellarator, figure 2.4 , has the advantage that one does not need to rely on the complexity of currents
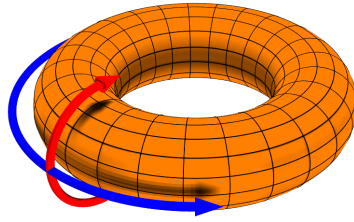
Figura 2.3: Torus. The blue arrow represents the toroidal direction and red the poloidal direction.

drives in order to avoid the losses to the containment. The losses are avoided by the fact that the planar cross sections are twisted in order to form a Möbius strip. This way, particles experiencing an upward drift in one side will be counterbalanced by a downward drift in the other side, creating an almost zero balance in the total drift.
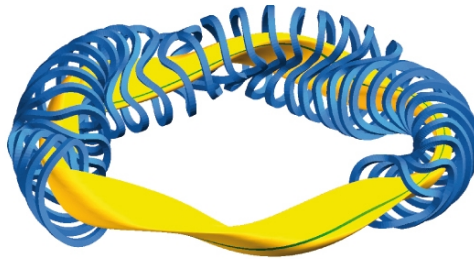
Figura 2.4: Stellarator design [credit: IPP]

Another solution to the drift problem is to bend the axial magnetic field lines in a poloidal direction, red line in figure 2.3, in this way, the field lines will created a flux surface rounding the whole torus, and a counteraction will be generated in order to avoid the drift losses. This approach is applied in the Tokamak reactors.

2.1.1   ITER and the tokamak model

Tokamak is the Russian acronym of the *ipsis litteris* "**to**roidal **ch**amber with **ma**gnetic **c**oils". The first prototype was proposed by leading scientist Lev Artsimovich in 1956. The tokamak is today the leading candidate design to reach the ignition and future economic feasibility in Nuclear Fusion. By using magnetic coils around the torus chamber, a toroidal magnetic field is generated in order to maintain the plasma confined. A second magnetic field, in the poloidal direction, is generated in order to bend the magnetic field lines, avoiding the magnetic gradient drift generated by the toroidal shape of the field. The latter field is generated by inducing a current in the plasma itself, following the principle of the Z pinch machine.

Following laser scattering measurements, and with the confirmation of the higher temperatures and stability of the tokamak model, the Joint European Torus (JET) began to be constructed in 1973. There are few operational tokamaks around the globe, one of them, the TCABR, can be found in the University of Sao Paulo, USP. The tokamak fast became the most used confinement approach around the world. The ITER, figure 2.5, latin for "*the way*", and acronym of ***International Thermonuclear Experimental Reactor***, started to be assembled in 2015, is the world largest MCF device. Expected to deliver fusion electricity by the end of 2030 (European Fusion Development Agreement, 2006).
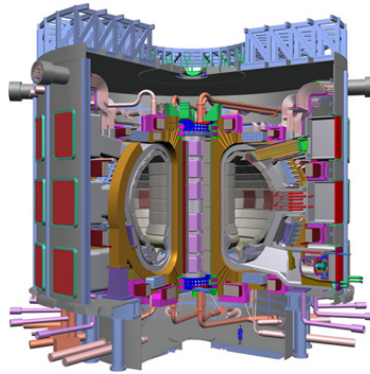
Figura 2.5: cross section view of the ITER [credit: iter.org].

The use of a current driven in the tokamak leads the plasma to a series of instabilities. Most of this instabilities are due to Magnetohydrodynamic (MHD) modes, *i. e.* this modes degraded the confinement and can lead to plasma disruption. Microturbulences driven by ions also contributes to plasma disruption scenario.

The full scenario of instabilities and degradation in ITER may be stabilized by a set of complex feedback controls that increase the complexity of the machine.

2.2 DYNAMICS IN MAGNETIZED PLASMA

In order to understand the dynamic of plasma confinement, and therefore toroidal confinement, one must first recall the orbit dynamic of particles under the influence of electric and magnetic fields. The *orbit theory* is used to study the dynamic of charged particles under the influence of electric and magnetic fields. It is very important first order description of plasma behavior. It does not take out the need for an improved statistic model, though, as the one used in the *Kinetic theory*. The Hamiltonian mechanism is used in order to describe the dynamic of the system in the space of the canonical coordinates and it can be used to elegantly describe the conservation of a property known as adiabatic invariant.

Let us consider the Lorentz equation for a particle with charge **q** under the action of a force $\vec{F}$ due to the electric and magnetic fields $\vec{E}$ and $\vec{B}$

$$\frac{dp}{dt} = F = \mathbf{q}(E + v \times B) \tag{2.1}$$

where $\vec{p}$ is the momentum of the particle and $\vec{v}$ its velocity. It is easy to see that under the influence of a electrostatic field, eq.2.1 results

$$r(t) = \frac{1}{2}\left(\frac{\mathbf{q}E}{m}\right)t^2 + v_0 t + r_0 \tag{2.2}$$

where r_0 is the initial position and v_0 is the initial velocity. In this case the particle has a constant acceleration, $\frac{\mathbf{q}E}{m}$. For a magnetostatic field the trajectory is found by separating the velocity of the particle in parallel and the perpendicular direction of the magnetic field. The movement in the direction of the magnetic field is not affected, and we are left with the perpendicular component of the resulting Lorentz equation

$$\frac{dv_\perp}{dt} = \frac{\boldsymbol{q}}{m}(v_\perp \times B) \tag{2.3}$$

considering $\Omega_c = -\frac{\boldsymbol{q}B}{m}$, and considering that Ω_c is constant in a constant magnetic field, known as cyclotron frequency, we can observe that 2.3 can be integrated to

$$v_\perp = \Omega_c \times r_c \tag{2.4}$$

where $\vec{r}_c$ is the the particle position related to the center of the gyration point, in a plane perpendicular to $\vec{B}$. Equation 2.4 represents the rotation of the position $\vec{r}_c$. The resulting motion of the particle is given by the superposition of the uniform motion along $\vec{B}$ and and the circular motion perpendicular to $\vec{B}$. The radius in which the particle gyro-rotates is known as Larmor radius, defined as $\rho = \frac{mv_\perp}{qB}$.

The analysis of $\vec{E}$ together with $\vec{B}$ is done by separating the components of $\vec{v}$ and $\vec{E}$ parallel and perpendicular to $\vec{B}$. In the same direction of the magnetic field, we have

$$r_\parallel(t) = \frac{1}{2}\left(\frac{\mathbf{q}E_\parallel}{m}\right)t^2 + v_\parallel(0)t + r_\parallel(0) \tag{2.5}$$

The perpendicular solution can be found by separating $v(t)$ in $v\prime(t) + v_E$, being v_E a velocity in the plane perpendicular to B. Decomposing the perpendicular electric field in

$$E_\perp = -\frac{E_\perp \times B}{B^2} \times B \tag{2.6}$$

one can finally arrive in the description of the particle motion unconstrained to a coordinate frame

$$v(t) = \Omega_c \times r_c + \frac{E_\perp \times B}{B^2} + \frac{\mathbf{q}E_\parallel}{m}t + v_\parallel(0) \tag{2.7}$$

In equation 2.7, the term $\frac{E_\perp \times B}{B^2}$ represents the $E \times B$ drift. The result motion of the particle is a cycloid.

It can be observed that, when E and B are perpendicular a confined plasma, a drift found in the second term on RHS of equation 2.7, is created. Thus a possible loss of material in the $v(t)$ direction is foreseen and the confinement may be terminated.

2.3 TOROIDAL CONFINEMENT

Toroidal confinement is of great importance because it was the chosen configuration in which most of the efforts to develop sustained nuclear power are put nowadays. Two important topics in toroidal confinement must be contemplated for the scope of this work, firstly, classical motion of particles in non uniform magnetic fields, and secondly, the equilibrium of forces in a toroidaly magnetized plasma.

2.3.1 Classical Analysis

An important consideration that must be done is the drift in slowly changing fields. In the case of a toroidally confined plasma, the geometry of the magnetic field does not allow it to have a continuous value in all the space. A drift is generated due to changes in the magnetic field intensity along the particle orbit.

First we need to consider the magnetic field, our object of study in this section, varying with the position vector in reference to the gyrocenter direction, $r_L(t)$. The motion of the particle is in the direction of the magnetic field, and the position and velocity vector can be decomposed in the gyrocenter direction, related to the field line, and around the field line.

$$B(x(t)) = B(x(t)) + r_L(t)) = B(x(t)) + (r_L(t)) \cdot \nabla)B \tag{2.8}$$

Using Taylor expansion in the Lorentz equations, we have

$$m\frac{\mathrm{d}[v_{gc}(t)+v_l(t)]}{\mathrm{d}t} = q[E(x_{gc}(t))+(r_l(t)\cdot\nabla)E]+q[v_{gc}(t)+v_l(t)]\times[B(x_{gc}(t)+(r_l(t)\cdot\nabla)B]$$

$$\text{(2.9)}$$

And the first cyclotron motion can be extracted as

$$m\frac{\mathrm{d}v_l(t)}{\mathrm{d}t} = qv_l\times B(x_{gc}(t)) \tag{2.10}$$

and

$$m\frac{\mathrm{d}v_{gc}(t)}{\mathrm{d}t} = q[E(x_{gc}(t))+(r_l(t)\cdot\nabla)E]+q[v_{gc}(t)\times[B(x_{gc}(t))+(r_l(t)\cdot\nabla)B]+v_l(t)\times(r_l(t)\cdot\nabla)B] \tag{2.11}$$

Now, decomposing the gyrocentric velocity in two perpendicular components

$$v_{gc}(t) = \left\{ \begin{array}{c} v_{\perp gc}(t) \\ v_{\parallel gc}(t)B \end{array} \right\} \tag{2.12}$$

The time derivative of the left hand side of 2.12 is taken as the sum of the two components in the right hand side. Form here, a relation to the derivative of the magnetic field direction can be taken

$$\frac{\mathrm{d}B}{\mathrm{d}t} = \frac{\partial B}{\partial s}\frac{\mathrm{d}s}{\mathrm{d}t} = v_{\parallel gc}(t)B\cdot\nabla B \tag{2.13}$$

Where s represents a field element line. We can, now, decompose Lorentz equation along and perpendicular to B

$$m\frac{\mathrm{d}v_{\parallel gc}(t)}{\mathrm{d}t} = q\left[E_{\parallel}(x_{gc}(t))+\langle v_l(t)\times(r_l(t)\cdot\nabla)B\rangle_{\parallel}\right] \tag{2.14}$$

and for the perpendicular direction

$$m[\frac{\mathrm{d}v_{\perp gc}(t)}{\mathrm{d}t}+v_{\parallel gc}^2(t)B\cdot\nabla B] = q\left[\begin{array}{c} E_{\perp}(x_{gc}(t)) \\ +v_{gc}(t)\times B(x_{gc}(t)) \\ +\langle v_l(t)\times(r_l(t)\cdot\nabla)B\rangle_{\perp} \end{array}\right] \tag{2.15}$$

In a more generic form

$$m\frac{\mathrm{d}v_{\perp gc}(t)}{\mathrm{d}t} = F_{\perp}+qv_{gc}\times B \tag{2.16}$$

$\vec{F}_{\perp}$ being represented as

$$F_\perp = q \left[E_\perp(x_{gc}(t)) + \langle v_l(t) \times (r_l(t) \cdot \nabla)B \rangle_\perp \right] - m v_{\|gc}^2(t) B \cdot \nabla B \tag{2.17}$$

If we consider that $v_{\perp gc}(t)$ has a slow time dependence, we can approximate the perpendicular gyrocentric velocity

$$v_{\perp gc}(t) \simeq v_F \equiv \frac{F_\perp \times B}{qB^2} \tag{2.18}$$

Considering now an approximation to the first guess, $v_{\perp gc}(t) = v_F + v_P$ and developing based on the above assumption

$$m \frac{\mathrm{d}v_F + v_P}{\mathrm{d}t} = F_\perp + \mathbf{q}(v_F + v_P) \times B \tag{2.19}$$

and considering also that $\left| \frac{\mathrm{d}v_P}{\mathrm{d}t} \right| \ll \left| \frac{\mathrm{d}v_F}{\mathrm{d}t} \right|$ we arrive in the general polarization drift

$$v_P = -\frac{m}{qB^2} \frac{\mathrm{d}v_F}{\mathrm{d}t} \times B \tag{2.20}$$

In the case that we have $\vec{v}_F = \vec{E} \times \vec{B}$ the polarization drift becomes

$$v_P = -\frac{m}{qB^2} \frac{\mathrm{d}E}{\mathrm{d}t} \tag{2.21}$$

If, now, we consider the drift generated by the curvature of the magnetic field, one should just express how the perpendicular force is described in 2.18. Making a gyro average of the perpendicular force in cylindrical coordinates, we get

$$\langle F_\perp \rangle = -2|m|(\frac{1}{2\pi} \oint \frac{\partial B}{\partial r} r d\theta) = -|m|(\nabla B)_\perp \tag{2.22}$$

The grad B drift becomes, so

$$v_{\nabla B} = -\frac{|m|}{q} \frac{(\nabla B) \times B}{B^2} \tag{2.23}$$

Equation 2.23 has a dependence in the particle charge, which means that electrons and ions drift in opposite direction and generate a net electric current.

A centrifugal force associated with the movement of the particles is generate due to the shape of the field. The force has the following form

$$F_c = -\frac{m v_{\|gc}^2}{R} R \tag{2.24}$$

Equation 2.24 represents the force associated with the curvature of fields line, and when substituted in 2.18 we get

$$v_c = -\frac{1}{qB^2}\frac{mv_{\parallel gc}^2 R}{R} \times B \tag{2.25}$$

Where R is the radius of the curvature. In a *tokamak*, it will be associated with the major radius.

It is important to understand that, the transport study is directly connected with the type of confinement constraining the particles. As seen above, classical electrodynamics provides us with a rustic approximation to the study of particles behavior in confined plasmas, but the fluid like nature of the plasma makes the study of transport relatively more complicated. A deeper study of transport will be done in the next chapter. In the present one, we will restrict ourselves with a phenomenological first order approximation description of the particle dynamic.

2.3.2 Magnetic Equilibrium and the Grad Shafranov Equation

In order to achieve a sustained fusion reaction, an equilibrium between the plasma pressure and the toroidal magnetic field must be achieved. Notwithstanding the instabilities generated by the toroidal geometry, that further on will be discussed, an internal balance between the plasma pressure and the forces from the magnetic field must be met. Such behavior is described by the Grad Shafranov equation.

Consider the plasma pressure to be isotropic, which means that the pressure tensor can be reduce to a diagonal matrix, the plasma momentum equation can be reduced to

$$J \times B = \nabla P \tag{2.26}$$

Where J is the current density, B is the Magnetic field and P is the pressure. By considering J, B, and P represented by a single-valued function of Ψ, the poloidal magnetic flux function determined by each poloidal flux associated with individual flux surfaces, one may represent the force balance equation in terms of the new variable Ψ.

Before proceeding, some assumptions are made. P is constant along a magnetic field line. This assumption is important because, since P is represented as a function of Ψ, the latter must, also, be constant along a magnetic field line, and therefore, P can be expressed individually by Ψ.

$$\mathbf{B} \cdot \nabla P = \frac{dP}{d\Psi}\mathbf{B} \cdot \nabla\Psi = 0 \tag{2.27}$$

In the toroidal direction, the space derivative of P vanishes, and from the plasma current description, considering R the radial direction, Z the toroidal direction, and $f = RB_\phi(R, Z)$, we can write the R and Z components of the current in terms of f as

$$J_R = -\frac{1}{R}\frac{\partial f}{\partial Z} \tag{2.28}$$

and

$$J_Z = \frac{1}{R}\frac{\partial f}{\partial R} \tag{2.29}$$

and, considering 2.28 and 2.29 in $J_Z B_R - J_R B_Z = 0$, we have

$$\frac{\partial f}{\partial R}B_R + \frac{\partial f}{\partial Z}B_Z = 0 \tag{2.30}$$

Which means, $\mathbf{B} \cdot \nabla f = 0$, in other words, f can, also, be described as a function of Ψ.

Considering the balance in the R direction, using the proper terms to express the current density and magnetic field, and considering that P and f are functions of Ψ, one may arrive in

$$\Delta^*\Psi = -R^2\frac{dP}{d\Psi} - f\frac{df}{d\Psi} \tag{2.31}$$

described in another manner,

$$\frac{\partial^2\Psi}{\partial Z^2} + R\frac{\partial}{\partial R}(\frac{1}{R}\frac{\partial\Psi}{\partial R}) = -R^2\frac{dP}{d\Psi} - f\frac{df}{d\Psi} \tag{2.32}$$

Equation 2.32 is known as Grad Shafranov equation, and it is used in order to describe equilibrium conditions for axisymmetric toroidal magnetized plasmas. This equation is widely used in plasma simulation codes in order to minimize the value of the total energy of the plasma pressure and magnetic field system, and find a suitable magnetic geometry that satisfies stability.

2.4 KINETIC THEORY

In the study of gases, the kinetic theory is responsible for analyzing the particles behavior through a statistical point of view. Macroscopic effects may be extracted from microscopic phenomena. Some assumptions must be made, nevertheless. The particles are smaller than the whole system, they follow newton's law of motion and undergo specific collision processes depending on the approach taken. The random movement generates a Maxwellian distribution function suitable for a first order approximation of the system. In plasmas the scenario is similar.

The kinetic theory brings the microscopic effects of particles into the macroscopic world through the use of statistical tools. The averaging out of microscopic effects lead to statistic kinetic effects, and these may lead us further to a particle-fluid characterization of the plasma.

In this section, one may see how statistic tools help us to extract information from the microscopic system and which is the role of *Boltzmann* and *Vlasov* equation in the description of the plasma.

2.4.1 Distribution Function and Boltzmann Equation

Consider a 6 dimensional phase space containing the 3 coordinates of space, r, and 3 coordinates of velocities, v, of a finite number of particles in a volume $d^3r d^3v$. Describing the number of particle in such a infinitesimal section by $d^6N(r,v,t)$, the function that represents the statistical distribution is denoted by the the number of particles over the volume of the phase space.

It is worth to notice that macroscopic quantities such as number density and average velocity may be averaged out from the distribution function as follows

$$n(r,t) = \int f(r,v,t) d^3v \tag{2.33}$$

Where $f(r,v,t)$ is the distribution function of the particles and the integral symbol stands for a triple integral. The average velocity comes out as

$$u(r,t) = \frac{1}{n(r,t)} \int v f(r,v,t) d^3v \tag{2.34}$$

Under specific considerations, the distribution function describes the change in the observable parameter. The qualitative construction of such relation is describe as following.

Consider the acceleration $a = F/m$ generated by a force F, acting in the volume element in the phase space of the system. Such force will make the element move in the phase space. The geometry of the volume element will change after a time t to a state f' as

$$[f(r',v',t+dt) - f(r,v,t)] d^3r d^3v = 0 \tag{2.35}$$

Using Taylor series and considering that the Jacobian transformation of the phase space from $d^3r d^3v$ to $d^3r' d^3v'$ is $|J| = 1$, we arrive in

$$f(r + vdt, v + adt, t + dt) = f(r, v, t) + \left[\frac{\partial f(r, v, t)}{\partial t} + v \cdot \nabla f(r, v, t) + a \cdot \nabla_v f(r, v, t)\right] dt$$

(2.36)

Equation 2.36 can be rewritten as

$$\frac{\partial f(r, v, t)}{\partial t} + v \cdot \nabla f(r, v, t) + a \cdot \nabla_v f(r, v, t) = 0$$

(2.37)

Known as the Boltzmann equation in the absence of collisions.

For a better description of transport phenomena, interactions must be taken into account, the change in the phase space configuration due to collision modifies the aspect of the finite element, introducing or withdrawing particles from its interior. Since the total balance of particles is in principle unknown, a collisional operator, representing the rate of change of the main distribution function, is introduced in the equation.

$$\left[\frac{\delta f(r, v, t)}{\delta t}\right]_{coll} d^3 r d^3 v dt$$

(2.38)

The modified equation thus becomes

$$\frac{\partial f(r, v, t)}{\partial t} + v \cdot \nabla f(r, v, t) + a \cdot \nabla_v f(r, v, t) = \left(\frac{\delta f(r, v, t)}{\delta t}\right)_{coll}$$

(2.39)

It is important to remember that the collisional model above described is a roughly, but accurate, approach and that more rigorous description exists, *e.g.* the Fokker-Planck model.

2.4.2   Vlasov Equation

By taking into account electric and magnetic fields, a more precise approximation can be formulated.

The Vlasov equation is described as the partial differential collisionless Boltzmann equation in the presence of macroscopic electric and magnetic fields.

$$\frac{\partial f}{\partial t} + v \cdot \nabla f + \frac{1}{m}(F_{ext} + q(E + v \times B)) \cdot \nabla_v f = 0$$

(2.40)

Where F_{ext} accounts for any other external force and inside the parenthesis is the Lorentz force from electric and magnetic fields, that should meet the constrains of the Maxwell Equations.

2.5 A FIRST APPROACH TO TRANSPORT THEORY

The transport theory is responsible for the study of transfer of quantities between and within a set of systems or a given system. Mass, momentum, and energy are quantities frequently analyzed as macroscopic variables of interest in order to describe plasma dynamics.

From the previously described Boltzmann equation and the particle distribution function, one may, by means of solving the latter with the help of the former, arrive in a set of equations suitable to guide us in understanding how the transport phenomena occurs in magnetized plasma. The plasma *macroscopic transport equations* are extracted directly from the Boltzmann equation in form of *moments of the distribution function*. As a result we have a set of equations known as *moments of the Boltzmann equations*. This moments can be associated with conservation equations of mass, momentum and energy, the objects of study of this section.

2.5.1 Qualitative analysis of moments of Boltzmann equation

The moments of the Boltzmann equation arise as an attempt to extract macroscopic properties of the system by means of the distribution function and the Boltzmann equation. A way to do so is to take the average of the distribution function in the Boltzmann equation considering the phase space of the independent parameter of the physical variable in consideration. Suppose that a given physical quantity, $\zeta(v)$, is proposed to be studied by the method of moments. First, one should average it out by multiplying it by the Boltzmann equation and integrating it in all space of velocities, then dividing the result by the particle number density.

Consider the Boltzmann equation 2.39, multiplying it by $\zeta(v)$ and integrating over the space of velocities we get

$$\int_v \zeta \frac{\partial f}{\partial t} d^3v + \int_v \zeta v \cdot \nabla f d^3v + \int_v \zeta a \cdot \nabla_v f d^3v = \int_v \zeta \left(\frac{\delta f}{\delta t} \right)_{coll} d^3v \tag{2.41}$$

We now Independently analyze each of the terms. The first term can be rewritten as

$$\int_v \zeta \frac{\partial f}{\partial t} d^3v = \frac{\partial}{\partial t} \left(\int_v \zeta f d^3v \right) - \int_v f \frac{\partial \zeta}{\partial t} d^3v \tag{2.42}$$

Considering that $\zeta(v)$ does not depend on time, the last term vanishes and using the standard notation of averages, $\langle \zeta(v) \rangle$, and making use of 2.33:

$$\int_v \zeta \frac{\partial f}{\partial t} d^3v = \frac{\partial}{\partial t} (n \langle \zeta(v) \rangle) \tag{2.43}$$

For the second term, the part containing the divergence vanishes due to the configuration of the velocity in the space phase, and likewise $\nabla \zeta(v)$ vanishes, since it is independent of the space variable. The second term then becomes

$$\int_v \zeta v \cdot \nabla f d^3 v = \nabla \cdot (n \langle \zeta(v) \rangle) \tag{2.44}$$

The third term requires more attention. Assuming that the field of forces has divergence zero, i.e., the force component in a given direction is independent of the velocity in that same direction, and considering the expansion of the third term

$$\int_v \zeta \, a \cdot \nabla_v f \, d^3 v = \int_v \nabla_v \cdot (a \, \zeta \, f) \, d^3 v - \int_v f \, a \cdot \nabla_v \zeta d^3 v - \int_v f \, \zeta \, \nabla_v \cdot a \, d^3 v \tag{2.45}$$

From equation 2.45, the first term of the right-hand side is a sum of three triple integrals , and each of this triple integrals result in zero, and the first integral in the right-hand side becomes

$$\int_v \zeta \, a \cdot \nabla_v f \, d^3 v = -n \langle a \cdot \nabla_v \zeta \rangle \tag{2.46}$$

Bringing together the separate result of the three terms, one is able to retrieve the *general transport equation*,

$$\frac{\partial}{\partial t}(n \langle \zeta(v) \rangle) + \nabla \cdot (n \langle \zeta(v) \rangle) - n \langle a \cdot \nabla_v \zeta \rangle = \left(\frac{\delta}{\delta t}(n \langle \zeta(v) \rangle) \right)_{coll} \tag{2.47}$$

The right-hand side represents the rate in which collision modifies the quantity ζ and alter the exchange of value .

2.5.2 Mass conservation

From this general principle, one may derive important relations that are helpful to understand how transport takes place within the constrains previous established. By firstly considering $\zeta = m$, where m is the mass of a given species, we have

$$\langle \zeta \rangle = m \tag{2.48}$$

$$\langle \zeta v \rangle = m \langle v \rangle \equiv m \, \mathbf{u} \tag{2.49}$$

$$\nabla_v \zeta = \nabla_v \, m = 0 \tag{2.50}$$

Replacing these quantities in the general transport equation we have

$$\frac{\partial \rho_m}{\partial t} + \nabla \cdot (\rho_m \mathbf{u}) = S \tag{2.51}$$

Equation **??** is known as the *continuity equation*. The term ρ represents the mass density $n \cdot m$, $\mathbf{u}$ is the linear velocity, and S represents the collision term.

By considering a collisionless scenario, dividing 2.51 by the mass m, and multiplying the whole equation by the charge of the specie, one may arrive at the *conservation of the electric charge* equation

$$\frac{\partial \rho_m}{\partial t} + \nabla \cdot \mathbf{J} = 0 \tag{2.52}$$

Where $\rho = n \cdot q$ is the charge density and $\mathbf{J} = \rho \mathbf{u}$ is the current density.

2.5.3   Momentum conservation

The conservation of momentum is extracted in a similar way as the mass conservation. Here, a more throughout analysis must be done in order to consider the standard variable $\zeta = mv$, being $v = w + u$, where w is the random movement around the mean velocity, and $\langle w \rangle = 0$.

Considering the acceleration in terms of the force and the mass, each of the terms can be reduced to

$$\frac{\partial}{\partial t}(n \, \langle \zeta(v) \rangle) = \frac{\partial}{\partial t}(m \, n \, u) \tag{2.53}$$

$$\nabla_v (m \, n \, \langle w_i w_j \rangle) = -\nabla \cdot \overset{\longleftrightarrow}{\Psi} \tag{2.54}$$

$$n \, \langle F \rangle = -n(r,t) \, q(E \, + \, v \times B) \tag{2.55}$$

Where $\overset{\longleftrightarrow}{\Psi}$ is the dyadic of pressure generated by the friction arising from the random movements w_i and w_j of the particles in different layers of the plasma. After considering the constrictions relative to the assumptions made, one will arrive at the following conservation equation

$$n\,m\,\frac{Du}{Dt} = n\,q\,(E + u \times B) - \nabla \cdot \overleftrightarrow{\Psi} - \delta \qquad (2.56)$$

This is the *momentum conservation equation*. It roughly represents how the rate in change of momentum varies with the collision term δ.

2.5.4 Energy conservation

In a similar way as already considered, the energy transport equation can be extracted from the Boltzmann equation in a partial differential form. Here, the general quantity ζ is replaced by the particle kinetic energy $\frac{mv^2}{2}$. In this case we have to consider the velocity as a two component quantity, and treat each term separately

$$\frac{\partial}{\partial t}(n\,\langle \zeta(v) \rangle) = \frac{\partial}{\partial t}\left(\frac{N\,\overleftrightarrow{\Psi}}{2} + \frac{m\,n\,u^2}{2}\right) \qquad (2.57)$$

$$\nabla \cdot (n\,\langle \zeta(v) \rangle) = \nabla \cdot \left(Q\left(\frac{2+N}{2}\right)\overleftrightarrow{\Psi}u + \frac{mnu^2}{2}u\right) \qquad (2.58)$$

$$-n\,\langle a \cdot \nabla_v \zeta \rangle = -q\,n\,u \cdot E \qquad (2.59)$$

And the collision term is

$$\delta = -\left(\frac{\partial W}{\partial t}\right)_{coll} \qquad (2.60)$$

representing the rate in which the energy is transferred among particles by collision effects.

Here, N represents the dimensional number in which the dyadic of pressure is considered, for isotropic cases it is considered unit. The quantity Q is the heat flux, expressed as

$$Q = \int_v \frac{mw^2}{2}w\,f\,d^3v \qquad (2.61)$$

Bringing up all the terms together and performing the necessary adjustments, we have

$$\frac{N}{2}\frac{D\overleftrightarrow{\Psi}}{Dt} + \frac{2+N}{2}\overleftrightarrow{\Psi}\nabla \cdot u = -\nabla \cdot Q + \delta \cdot u - \left(\frac{\partial W}{\partial t}\right)_{coll} \qquad (2.62)$$

Where $\delta \cdot u$ represents the heating due to friction processes, and $\left(\frac{\partial W}{\partial t}\right)_{coll}$ the energy transferred by collision.

2.6 CONSIDERATIONS

From the equations above described, it is advantageous to compute two quantities, relating the moments extracted from the Boltzmann equation and the magnetic flux function, expressed in two important transport quantities in terms of the flux function Ψ.

$$\langle \Gamma \cdot \nabla \Psi \rangle = \left\langle \int_v d^3v f u \cdot \nabla \Psi \right\rangle \tag{2.63}$$

$$\langle Q \cdot \nabla \Psi \rangle = \left\langle \int_v d^3v \frac{m\, u^2}{2} f\, u \cdot \nabla \Psi \right\rangle \tag{2.64}$$

Equation 2.63 represents the flux surface average of the radial particle flux, 2.64 is the energy flux, and $\langle \cdot \rangle$ denotes flux surface average.

Having derived the most important moments of the Kinetic Theory from the Boltzamnn equation, we notice that this set of partial differential equations describe how the movement of mass, momentum and energy shall occur but it is important to observe that this model is a simple representation of the classical transport expected in a Toroidaly confined plasma. A better description of the plasma physics must be done in order to better foresee tokamak plasma dynamics.

3 TOKAMAK

3.1 REALISTIC TRANSPORT MODELS

It is important to observe that, although elegantly derived from fluid dynamics and electromagnetic theory, the classical models of transport are not enough to describe the dynamics of the particles in a tokamak. The consideration of the toroidal magnetic geometry of the device plays an important role in most recent models, where effects due to the gradients of the field start to show the importance and impact of morphological considerations.

3.1.1 Classical Transport Operators

The former Vlasov equation needs to be modified in the sense that it must now account for effects like collisions. Classical and collision induced plasma current must be defined and irreducible levels of transport caused by Coulomb collision must be included. Two operators are considered. The Fokker-Planck coulomb collision operator makes the assumption that particles can only collide with each other and with other particles, bringing us to a rate change in the distribution function due to internal collisions, expressed as

$$C(f) \equiv \left(\frac{\partial f}{\partial t}\right)_{\Delta v} = \lim_{\Delta t \to 0} \frac{f(x,v,t) - f(x,v,t-\Delta t)}{\Delta t} \tag{3.1}$$

The integro-differential form of the operator can be described as as

$$C(f) \cong -\frac{\partial}{\partial v} \cdot \frac{\langle \Delta v \rangle}{\Delta t} f + \frac{1}{2}\frac{\partial^2}{\partial v \partial v}\frac{\Delta v \Delta v}{\Delta t} f + ... \tag{3.2}$$

The Operator is a scalar, invariant under rotation, and symmetric with respect to Galilean transformations, making it a rotationally symmetric, or isotropic, operator. When expressed in terms of the Rosenbluth Potentials, from the Rosenbluth-MacDonald-Judd form, and considering the specific changes in velocity vector due to coulomb collisions of particle "a"with background particle "b", one may get the form

$$C(f) = -\frac{\partial f}{\partial v} \cdot \Gamma_{ab}\frac{\langle \partial H_b \rangle}{\partial v} f + \frac{1}{2}\frac{\partial^2}{\partial v \partial v}\Gamma_{ab}\frac{\partial G_b}{\partial v \partial v} f \tag{3.3}$$

Where H_b and G_b represent the Rosenbluth potentials

$$H_b(v) = (1 + \frac{m_a}{m_b})\int d^3v' \frac{f_b(v')}{|v-v'|} \tag{3.4}$$

$$G_b(v) = \int d^3v' f_b(v')|v - v'| \tag{3.5}$$

And the factor Γ is represented as

$$\Gamma = \frac{q_a^2 q_b^2 ln(\Lambda_{ab})}{4\pi\epsilon_0 m_a^2} \tag{3.6}$$

Where $ln(\Lambda_{ab})$ is the Coulomb logarithm. Another important consideration that must be done in regard to the collision of particles with a stationary background, is the Lorentz Collision Operator expressed as:

$$C_L(f) = \frac{\nu(v)}{2}\left[\frac{\partial}{\partial\zeta}(1 - \zeta^2)\frac{\partial f}{\partial\zeta} + \frac{1}{1 - \zeta^2}\frac{\partial^2 f}{\partial\varphi^2}\right] \tag{3.7}$$

Where $\zeta = \frac{v_\parallel}{v}$ and $\varphi = tan^{-1}\frac{v_y}{v_x}$. For $\frac{\langle\Delta v\rangle}{\Delta t} = \nu(v)v$. This operator might be seen as a form of angular scattering in the velocity space.

From now on, one must be capable of recognizing important factors and a more precise description of a tokamak plasma transport.

3.1.2 Electrical Conductivity within Lorentz operator

An important property that must be studied in order to precisely describe plasma inner mechanisms is known as electrical conductivity. The electrical conductivity help us to quantify a material's ability to allow transport of electric charges, be it electrons or ions. Following the Spitzer-Härm argument, the study of plasma conductivity is done by assuming the application of a Electrical field E in an infinite homogeneous plasma and analyzing its steady state current. Something with the form $\mathbf{J} = \sigma\mathbf{E}$ is expected, being σ the conductivity. Making use of the Vlasov equation for the Maxwellian distribution function, one may get

$$\frac{q}{m}E \cdot \frac{\partial f}{\partial v} = C(f) \tag{3.8}$$

From a phenomenological point of view, a correct scaling with plasma parameters is found when we consider the electron momentum balance and a shifted maxwellian distribution. Integrating 3.8 in $\int mvd^3v$, resulting in $-nqE - mn\nu v$, we get

$$J = -nqv = \frac{nq^2}{m\nu}E = \sigma E \equiv \frac{E}{\eta} \tag{3.9}$$

the first order approximation of the plasma electrical conductivity is

$$\sigma_0 = \frac{nq^2}{m\nu} \tag{3.10}$$

Any improvement in this conductivity will only add numerical coefficients to the very same value represented above, preserving the former scaling.

Consider, for instance, the Lorentz collision model. Expanding the electron distribution function for small E, we have $f_e = f_0 + \epsilon f_1$, where $\frac{E}{E_{crit}} << 1$.

$$\epsilon^1 : C_L(f_1) \rightarrow \frac{evEf_m}{T_e}\zeta = \frac{\nu(v)}{2}\frac{\partial}{\partial\zeta}(1-\zeta^2)\frac{\partial f_1}{\partial\zeta} \tag{3.11}$$

Where we consider that for $\epsilon^0 : f_0 = f_m(v)$, and f_m is the maxwellian distribution. Using the Legendre polynomial series $f_1(v,\zeta) = \sum_{n=0}^{\infty} f_{1,n}(v)P_n(\zeta)$, and using just the first term for this approximation

$$f_e(v) \cong f_m(v)\left[1 - \frac{qv\zeta E}{T_e\nu(v)} + ...\right] \tag{3.12}$$

We have, therefore

$$J = -\int d^3v qv f_e \equiv \sigma E \tag{3.13}$$

And so

$$\sigma_L = \frac{32}{3\pi}\frac{nq^2}{m\nu} \tag{3.14}$$

The increased observed in the Lorentz approximation for the electrical conductivity is due to high energy electrons with lower collision frequency. A numerical solution found by Spitzer gives us $\sigma_{Sp} = \frac{1}{\alpha}\frac{nq^2}{m\nu}$, being α a parameter dependent of the atomic number of the ions, ranging from 0.51 for $Z_i = 1$ to 0.29 for $Z_i \rightarrow \infty$.

3.1.3 Random walk approach

A random walk consists of a movement that in principle has no determined pattern, and it is random by definition (D. Ben-Avraham, 2000). It is expressed as a succession of random steps. Note that in this model, the true causal deterministic or non deterministic nature of the process *per se* is not discussed. By using this argument, we are capable of deducing some transport coefficients perpendicular to the magnetic field B.

The randomness of the walk comes from collision of particles in their gyromotion orbits. The diffusion coefficient is described as $D \sim \frac{\langle (\Delta x)^2 \rangle}{\Delta t} \sim \rho^2 \nu$. Any step with size comparable to ρ is considered a classical transport.

It is interesting to notice that collision of alike particles does not lead to particle diffusion, $D_{\perp ee} = D_{\perp ii} = 0$, but do lead to heat diffusion $\chi_{\perp ee} \sim \nu_{ee} \rho_e^2$, and $\chi_{\perp ii} \sim \nu_{ii} \rho_i^2$. Collisions of unlike particles can lead to heat and particle diffusion, as expressed in $D_{\perp ei} \sim \nu_{ei} \rho_e^2$, and $\chi_{\perp ei} \sim \nu_{ei} \rho_e^2$. The classical perpendicular transport is the net sum of these various processes. For electrons we have

$$D_{\perp e} = D_{\perp ei} \sim \nu_{ei} \rho_e^2 \tag{3.15}$$

$$\chi_{\perp e} = \chi_{\perp ee} + \chi_{\perp ei} \sim (\nu_{ee} + \nu_{ei}) \rho_e^2 \tag{3.16}$$

And for the ions we have a similar situation,

$$D_{\perp i} = D_{\perp ei} \sim \nu_{ei} \rho_e^2 \tag{3.17}$$

$$\chi_{\perp i} = \chi_{\perp ii} + \chi_{\perp ie} \sim \nu_{ii} \rho_i^2 \tag{3.18}$$

It is easy to observe that since $D_{\perp e} = D_{\perp i}$, the perpendicular transport is ambipolar, and no charge separation is generated.

Parallel to B, in a similar way, the transport coefficients can also be determined. We must consider here that the step size is related to the mean free path of the particle, $\lambda = \frac{v_T}{\nu}$, consequently, for the electron-electron case

$$\chi_{\parallel ee} \sim \nu_{ee} \lambda_e^2 \sim \frac{v_{Te}^2}{\nu_e} \tag{3.19}$$

$$D_{\parallel ee} = 0 \tag{3.20}$$

For the ion-ion case

$$\chi_{\parallel ii} \sim \nu_{ii} \lambda_i^2 \sim \frac{v_{Ti}^2}{\nu_i} \tag{3.21}$$

$$D_{\|ii} = 0 \tag{3.22}$$

The electron-ion case is expressed as

$$\chi_{\|ei} \sim \nu_{ei}\lambda_i\lambda_e \sim \frac{v_{Ti}^2}{\nu_i} \tag{3.23}$$

$$D_{\|ei} \sim \frac{v_{Ti}^2}{\nu_i} \tag{3.24}$$

We also have for Electrons

$$D_{\|e} = D_{\|ei} \sim \frac{v_{Ti}^2}{\nu_i} \tag{3.25}$$

$$\chi_{\|e} \sim \nu_e\lambda_e^2 \tag{3.26}$$

And for Ions

$$D_{\|i} = D_{\|ei} \sim \frac{v_{Ti}^2}{\nu_i} \tag{3.27}$$

$$\chi_{\|i} \sim \nu_{ii}\lambda_i^2 \tag{3.28}$$

Observe that, for a first order approximation where ions and electrons have the same temperature, perpendicular transport is highly dominated by Ion Heat Diffusion, but the parallel transport is, differently, dominated by electron heat diffusion. The parallel heat transport, in this scenario, can be up to thousands times larger than perpendicular heat transport.

3.1.4   The Braginskii equations

For a collisional and magnetized plasma, the Chapman-Enskog method, firstly thought for a general gas, is an interesting approach in which a small parameter ϵ, related to the collisional time and macroscopic time scale, is used in order to solve the kinetic equation and compute transport parameters. When assumed to be Maxwellian, the distribution function gives us a clear and elegant collision operator, and assumes $T_e = T_i$ and $V_e = V_i$. At this point, one could expand the distribution function via momentum, and arrive at the following relation

$$f = f_n[1 + \frac{2}{v_T^2} \cdot v \left[u_0 L_0^{3/2} + u_1 L_1^{3/2} \right] + 2\frac{v \cdot v - (v^2/3)I}{mnv_T^4} : [\Pi_0 L_0^{(5/2)} + \Pi_1 L_1^{(5/2)}] + ...] \quad (3.29)$$

For the first term in the right hand side, one has the lowest order Mawxellian term, the second and third terms are proportional to ϵ and ϵ^2 respectively. Following the moment approach to the Spitzer problem, the moments of kinetic equation $\int d^3v m v L_i^{3/2}$ and $\int d^3v (vv - \frac{v^2}{3}I) L_i^{5/2}$ gives us a coupled set of equations for u_0 and Π_0 and its higher order complements. The multiplication of this set of equations by the friction coefficient matrices gives us the parameters related to the flow, u, and stress, Π.

The zeroth order of the conservation equations originated from the above description can be listed. First, considering that the Fokker-Planck collision operator for conserved particles, we have for the density

$$\frac{\partial n_s}{\partial t} + \nabla \cdot (n_s u_s) = 0 \quad (3.30)$$

Where $n_s = \int f_s d^3v$ and $u_s = \frac{1}{n_s} \int f_s v d^3v$, are the density and averaged velocity. For the momentum conservation case, one would get

$$m_s n_s \frac{Du_s}{Dt} = Z_i e n_s (E + u_s \times B) - \nabla p_s - \nabla \cdot \Pi_s + R_{s,s'} \quad (3.31)$$

In the right hand side, we find terms corresponding to the Lorentz force, pressure, viscous force and frictional forces, respectively. The same path could be followed in order to demonstrate the respective equations for Energy and heat flux conservation. It is interesting to point out that, for the case of flux conservation, a parallel, crossed (diamagnetic), and perpendicular components are found, for the ionic case we have

$$q_i = -k_{\parallel i} b(b \cdot \nabla) T_i + k_{\Lambda i} b \times \nabla T_i - k_{\perp i} \nabla_\perp T_i \quad (3.32)$$

The relations for $k's$ are found to be $k_{\parallel s} \sim n_s \nu_s \lambda_s^2$, $k_{\Lambda s} \sim \frac{\nu_s}{\omega_s} k_{\parallel s}$, and $k_{\perp s} \sim n_s \nu_s \rho_s^2$.

It is worth to mention that the collisional entropy can be extracted from the Bragisnkii equations just by taking in consideration the electron entropy equation $S_e \equiv \frac{3}{2} \ln(p_e/n_e^{5/2})$, and $u = v_e - v_i$

$$\frac{\partial n_e S_e}{\partial t} + \nabla \cdot (S_e n_e v_e + \frac{q_e}{T_e}) + \frac{Q_{ei}}{T_e} = -\frac{1}{T_e}[q_e \cdot \nabla \ln T_e + \frac{1}{2}\Pi_e : \nabla v_e + R_e u] \quad (3.33)$$

From the above equation we are capable to observe terms related to convection and conduction, or entropy flow, on the left hand side, and on the right hand side dissipation processes such as heat transport, viscous heating and flow heating.

Despite of its robustness, the Braginskii equations possess some worth to comment preliminary limitations, mainly regarded to real case tokamaks. The parallel and perpendicular gradient scale lengths of macroscopic quantities must be large in comparison to the collision mean free path and gyroradius, respectively. Macroscopic quantities have, also, a moderated rate of change when compared to collision frequency. Small scale processes may appear, but they are averaged out from the net transport, they would have to, then, be described by kinetic characterization and then added to the Braginskii's equations.

If we consider the balance equations, with a gradient of the temperature equals zero and $E = E^A - \nabla\phi$, we are capable of determining flows characteristic to classical transport and its coefficients for magnetized plasmas.

From equation **??**, we can arrive in the following relation

$$mn\frac{dV}{dt} = nq(E^A - \nabla\phi + V \times B) - \nabla p - \nabla \cdot \Pi - nq\left(\frac{J_\parallel}{\sigma_\parallel} + \frac{J_\perp}{\sigma_\perp}\right) \tag{3.34}$$

From the above equation, a perpendicular, parallel and cross component to the flow may be extracted. The parallel flow is determined by

$$mn\frac{dV_\parallel}{dt} = nq(b \cdot E^A - b \cdot \nabla\phi) - b \cdot \nabla p - b \cdot \nabla \cdot \Pi - nq\frac{J_\parallel}{\sigma_\parallel} \tag{3.35}$$

Consider b to be equal to $\frac{B}{|B|}$, the $E \times B$ and diamagnetic flows are retrieved as a first order approximation of the perpendicular flows. For a first order perturbation approximation of ϕ and p, one gets

$$V_{\perp,1} = \frac{1}{B^2}B \times \left(\nabla\phi_0 + \frac{1}{nq}\nabla p_0\right) \tag{3.36}$$

$$J_{\perp,1} = \sum nqV_{\perp,1} = \frac{1}{B^2}B \times \nabla(p_e + p_i) \tag{3.37}$$

The equations of the perpendicular transport flows are extracted from the perpendicular components in higher orders

$$V_{\perp,2} = \frac{1}{nqB^2} B \times (mn\frac{dV_\perp}{dt} + \nabla \cdot \Pi + \frac{nq}{\sigma_\perp} J_{\perp,1}) + \frac{1}{B^2} B \times (\nabla\phi_1 + \frac{1}{nq}\nabla p_1) + \frac{1}{B^2} E^A \times B \quad (3.38)$$

Where the sum of the second, forth and fifth terms of the right hand side give us coefficients related to neoclassical transport, and the third is related to classical transport. while the last one is related to grid velocity.

$$J_{\perp,2} = \frac{1}{B^2} B \times \left(\rho_m \frac{dV_{\perp,i}}{dt} + \sum_s \nabla \cdot \Pi_s + \nabla \sum_s p_{1,s} \right) \quad (3.39)$$

In the classical transport due to friction between diamagnetic flows the classical diffusion is equal to $D_{cl}\nabla \ln n$, where $D_{cl} = \frac{T_e+T_i}{2T_e}\nu_e\rho_e^2$.

From the balance equations, a peculiar set of equations with important characteristics are extracted. Consider an axisymmetric geometry, where

$$B = I\nabla\zeta + \nabla\zeta \times \nabla\Psi \quad (3.40)$$

and,

$$\frac{\nabla\Psi \times B}{B^2} = -I\frac{B}{B^2} + R^2\nabla\zeta \quad (3.41)$$

In a tokamak geometry, consider also that the axisymmetric condition bring us the following considerations

$$\langle A \rangle \equiv \frac{\oint \frac{dl}{B} A(l)}{\oint \frac{dl}{B}} \quad (3.42)$$

and,

$$\langle B \cdot \nabla f \rangle = 0 \quad (3.43)$$

From the parallel momentum balance, expressed in equation 3.35, we have

$$0 = nq(B \cdot E^A - B \cdot \nabla\phi_1) - B \cdot \nabla p_1 - B \cdot \nabla \cdot \Pi - nq\frac{J_\parallel B}{\sigma_\parallel} \quad (3.44)$$

The particle flux can be reduced to

$$\Gamma_\Psi \equiv \langle V_{\perp,2} \cdot \nabla\Psi \rangle \quad (3.45)$$

Considering the description of $V_{\perp,2}$ here exposed, one may arrive in the following relations

$$\Gamma_{\Psi}^{neo} = -\frac{I}{q} \left\langle \frac{1}{B^2} \left[nq(B \cdot \nabla)\phi_1 + (B \cdot \nabla)p_1 + B \cdot \nabla \cdot \Pi \right] \right\rangle \tag{3.46}$$

$$= nI \left\langle \left(\frac{1}{B^2} - \frac{1}{\langle B^2 \rangle} \right) \left(\frac{J_\| B}{\sigma_\|} - E_\|^A B \right) \right\rangle + \frac{nI}{\langle B^2 \rangle} \left\langle \frac{J_\| B}{\sigma_\|} - E_\|^A B \right\rangle \tag{3.47}$$

The first bracket represents the Pfirsch-Schlüter transport, within the flux surface, and the second one, averaging the flux surface, the Banana-Plateau.

The total current within the flux surface, considering the charge continuity equation, is found to be

$$J_\| B = -I \frac{d}{d\Psi}(p_e + p_i)(1 - \frac{B^2}{\langle B^2 \rangle}) + \frac{\langle J_\| B \rangle B^2}{\langle B^2 \rangle} \tag{3.48}$$

The first term in the right hand side is the Pfirsch-Schlüter current, resulting in a diffusive flux $\Gamma^{PF} \sim q^2(\Psi)D_{CL}$ and larger than the classical diffusion values.

Albeit complete and rigorous, classical, mostly perpendicular, transport, does not account for the experimental measurement (K.Tanaka, 2007). Banana orbits and instabilities fluctuations may yet play a significant role and must be taken into account. A generalization of the Braginskii equations for any ratio of mean free path to gradient lengths must be done as well as losses processes in the case of open field lines and better accounting for effects of viscosity must be.

3.1.5 Neoclassical Transport

The neoclassical description comes in order to improve the outdated and mismatched classical model and attempt to fill the gaps of divergences between classical predictions and real measurements.

Perpendicular diffusion can be estimated with the random walk argument and is directly related to the Banana regime, where $D \sim \nu \rho^2 q^2 / \epsilon^{3/2}$ is phenomenologically described. Depending on the collision frequency, the bananas orbits may be completed or not, arriving to the point of drift off from the flux surface, where $D \sim w_b \rho^2 q^2 / \epsilon^{3/2}$, and w_b is the untrapped particle bounce frequency. In the highest collision frequency cases, Pfirsch-Schlüter Diffusion dominates with $D \sim \nu \rho^2 q^2 / \epsilon^{3/2}$, and $\nu >> w_b$.

In neoclassic processes, ion perpendicular heat transport takes an important role, and it dominantly affects the whole transport. Perpendicular transport is highly scaled with collisionality, going from banana to Pfirsch-Schlüter regime depending on ν as seen in figure 3.1. Electrical
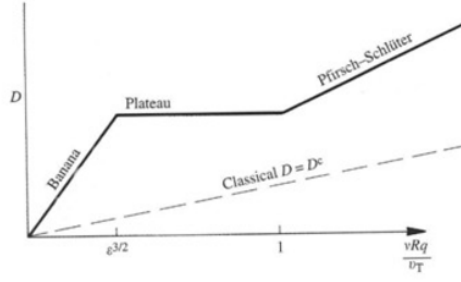
Figura 3.1: Diffusion level as function of collisionality regime [reference:Jan Mlynar]

conductivity is decreased due to trapped particle effects and the Bootstrap current, the parallel component of viscous damping of poloidal electron diamagnetic flow and an important neoclassical prediction, arises. Effects on viscous damping of poloidal flows, where untrapped particles carry flow and collide with stationary trapped particles, are also observed.

Bootstrap current is driven by density and temperature gradient. It is independent of other current drive mechanisms and provide most of the poloidal field in the advanced tokamak scenarios.

By applying the Braginskii theory in the framework of neoclassical transport, generalizing parallel viscous stress, and some limitations, we can modify Π in order to have a better description of the banana-plateau regime .

$$\Pi = \Pi_\parallel + \Pi_\Lambda + \Pi_\perp \tag{3.49}$$

Where $\Pi_\parallel$ is the divergent in the banana-plateau regime and the other two terms in the RHS are negligible when compared to the first term. Making use of the Chew-Goldberger-Low description, we have $\Pi_\parallel = (p_\parallel - p_\perp)(bb - I/3)$, considering again $b = B/|B|$. The anisotropic pressure of first degree is generated due to flow against ∇B, and is related to the viscous damping frequency μ, directly dependent on the collisionality regime.

$$p_\parallel + p_\perp \approx \frac{-mn\mu \langle B^2 \rangle}{\langle (b \cdot \nabla B)^2 \rangle} V \cdot \nabla \ln B \tag{3.50}$$

Viscous forces due to parallel viscous stress are of high importance in the description of the banana orbits, since they play a direct role in the flux transport. The parallel component of the force can be described as

$$B \cdot \nabla \cdot \Pi_\parallel = -(p_\parallel - p_\perp)(b \cdot \nabla)B + \frac{2}{3}(B \cdot \nabla)(p_\parallel - p_\perp) \tag{3.51}$$

The flux surface averaged force gives us a picture of the effects of viscosity in the damping of poloidal flows, and is described by using the magnetic field in poloidal coordinates:

$$\langle B \cdot \nabla \cdot \Pi_\| \rangle = mn\mu u_\theta \langle B^2 \rangle \tag{3.52}$$

Where

$$u_\theta(\Psi) = \frac{V_\theta}{B_\theta} = \frac{V_\|}{B} + \frac{I(\Psi)}{B^2}\left(\frac{\partial\phi}{\partial\Psi} + \frac{1}{nq}\frac{\partial p}{\partial\Psi}\right) \tag{3.53}$$

And its effect on poloidal flows is observed by using Newton's second law on $\langle V_\| B \rangle$, and cosidering μ as the parallel poloidal flow damping frequency.

$$mn\frac{d}{dt}\langle V_\| B \rangle = -mn\mu u_\theta \langle B^2 \rangle \tag{3.54}$$

The parallel poloidal ion flow can also be determined by the momentum balance. Assuming that the gradient of the temperature is zero, from Newton's second law and summing over the plasma species, one may have

$$0 = B \cdot \nabla \cdot (\Pi_{\|e} + \Pi_{\|i}) \sim -m_i n_i \mu_i U_{\theta i}(\Psi) \langle B^2 \rangle 2\sin^2\theta \tag{3.55}$$

Leading us ultimately to

$$0 = U_{\theta i}(\Psi) \sim \frac{V_\|}{B} + \frac{1}{BB_\theta}\left(\frac{d\phi_0}{dr} + \frac{1}{n_i q_i}\frac{dp_{i0}}{dr}\right) \tag{3.56}$$

A resultant flow in the toroidal direction, when in equilibrium, damped on perpendicular transport time scale is brought in association with the toroidal angular rotation frequency

$$w(\Psi) \equiv V \cdot \nabla\zeta = -\left(\frac{d\phi_0}{d\Psi} + \frac{1}{n_i q_i}\frac{dp_{0i}}{d\Psi} - \frac{1.17}{q_i}\frac{dT_{i0}}{d\Psi}\right) \tag{3.57}$$

Where the value 1.17 is the correct value for a banana regime, in the case where the gradient of the temperature is different of zero. The toroidal velocity can be approximated as

$$V_\zeta \sim -\frac{1}{B_\theta}\left(\frac{d\phi_0}{dr} + \frac{T_{i0}}{n_i q_i}\frac{dn_{i0}}{dr} - \frac{0.17}{q_i}\frac{dT_{i0}}{dr}\right) \tag{3.58}$$

Ohm's Law is easily worked out in the framework of parallel electron momentum. In a similar approach, using $\nabla T = 0$, and considering the parallel momentum of electrons, we have

$$\langle J_\| B \rangle = \sigma_\| \langle E_\|^A B \rangle + \frac{\sigma_\|}{n_e e}\langle B \cdot \nabla \cdot \Pi_{\|e} \rangle \tag{3.59}$$

The last term will become something similar to equation 3.55, and the poloidal flow velocity, $U_{\theta e}$, can be solved from the solution of the electron ion momentum balance. A resultant Ohm's

law from the flux surface averaged is

$$\left\langle B J_\parallel \right\rangle = \frac{\sigma_\parallel \left\langle E_\parallel^A B \right\rangle}{1 + \mu_e/\nu_e} - \frac{\mu_e/\nu_e}{1 + \mu_e/\nu_e}\left[I\frac{d(p_e + p_i/Z_i)}{d\Psi} - n_e e U_{\theta i}\left\langle B^2 \right\rangle \right] \tag{3.60}$$

The effects of trapped particles on electrical conductivity, due to viscosity effects, as well as the Bootstrap current, due to viscous drag on poloidal electron diamagnetic flow, can be extracted if one considers $\mu_e/\nu_e \sim \sqrt[2]{\epsilon}$, $U_{\theta i} \sim 0$, and $d\Psi \sim B_\theta R dr$. An interesting result in the frame of radial particle flux in neoclassical Banana-Plateau regime is the ware pinch flux, that come as a result of the consideration of poloidal electron flow in the radial particle flux component, it is characterized by $W = I\mu_e/\nu_e \left\langle E_\parallel^A B \right\rangle$

The total neoclassical transport is obtained by putting together Classical, Banana-Plateau, and Pfirsch-Schlüter transports.

$$\Gamma = \left\langle n V \cdot \nabla\Psi \right\rangle = \left\langle \frac{1}{B^2}\nabla\Psi \cdot B \times \left(\frac{nqJ_\perp}{\sigma_\perp} + nq\nabla\phi_1 + \nabla p_1 + \nabla \cdot \Pi_\parallel \right) \right\rangle \tag{3.61}$$

Where the first term inside the right-hand-side parenthesis accounts for the classical transport, and the last three terms for Pfirsch-Schlüter and Banana-Plateau transport. In a reduced matrix form, the flux surface averaged neoclassical transport equations can be shown as

$$\begin{pmatrix} \Gamma \\ q_e \\ J_\parallel - \sigma_\parallel E_\parallel^A \end{pmatrix} = -\begin{pmatrix} D_e & L_{12} & W \\ L_{21} & \chi_e & L_{23} \\ B & L_{32} & \sqrt[2]{\epsilon}\sigma_\parallel \end{pmatrix}\begin{pmatrix} dn/dr \\ dT_e/dr \\ E_\parallel^A \end{pmatrix} \tag{3.62}$$

Consider $q_i = -n\chi_i dT_i/dr$, $D_e \sim \chi_e$ in the neoclassical approach, and the right-hand-side of equation 3.62 the linkage between the transport components and thermodynamic forces.

Aspects related to impurity tendency to peak at certain regions of the torus, radial ambipolar transport and nonaxisymmetric toroidal Magnetic field ripple can also be extracted from the neoclassical transport approach

3.2 ANOMALOUS MECHANISMS

Notwithstanding the advances brought in neoclassical tokamak transport theory, diverse anomalous effects are found when some of the flux parameters are contrasted with real experimental measurements. From the various discrepancies, processes related to electron heat diffusivity, particle diffusion, and electron runaway diffusion seems to be the most attenuated ones.

Perpendicular Ion heat transport in large tokamaks seems to be the most troublesome parameter, together with perpendicular electron heat and particle transport. The idea to develop a more complete set of equations for any degree of collisionality brings us to the development of a class of transport phenomena called Anomalous Transport, responsible to describe the discrepancy between experimental and neoclassical transport.

4 ANOMALOUS TRANSPORT

It is found that measurements of transport levels in tokamaks exceeds the values predicted by the neoclassical theory. Due to the excess in transport levels, neoclassical transport is hardly properly tested. A new model must be developed in order to match the experimental transport levels measured.

Anomalous transport is the theory responsible to quantify and study the additional part of the transport measured in magnetic confined plasmas. It is found to be driven mostly by turbulence and micro-instabilities (A.J.Wootton, 1990). In this chapter, we are going to examine the elemental foundations of the anomalous transport theory, and understand how this framework of study can, later, be used to solve accurate numerical problems that meets the expected transport levels.

4.1   THE NEW TRANSPORT MECHANISM

4.1.1   Bohm Diffusivity

After it was observed that the divergence of flux levels was enough to disturb precise prediction of the neoclassical theory, the study of the new transport mechanism led to the establishment of the Bohm diffusion as determined by anomalous processes. The Bohm diffusion coefficient is characterized by the following proportionality:

$$D^{(B)} \simeq \frac{K_B T}{eB} \tag{4.1}$$

Here, it is easy to observe the relation of the diffusion to the magnetic field strength B and the temperature T. It is important to observe that the level of transport is, therefore, determined by empirical observations.

It is argued that the main responsible for the anomalous level of transport divergence from neoclassical predictions is turbulence generated by micro-instabilities. It is easy to accept this argument when one acknowledges the reduction to neoclassical levels of transport when self-organization plays a role in the formation of H-modes and Internal Transport Barriers, later discussed.

4.1.2 The role of Turbulence

Turbulence is thought to be the mechanism in which fluids dissipate energy input from large scales to small scales, releasing it in the form of heat. The apparent random behavior of turbulent flows does not necessarily means that it is not deterministic, and therefore, a mathematical approach can be developed in order to comprehend the mechanism (Ben Dudson, 2014).

In magnetically confined plasmas, the role of turbulence is also understood as a way to dissipate the energy from the larger scales to the small ones, in form of micro-instabilities. The turbulent regime is characterized by small fluctuations in the mean plasma parameters, such as pressure, electric field and temperature. In this case, the energy is passed from larger scales to small ones, through cascades, where the energy can be finally released in the form of heat, as schematized in figure 4.1.
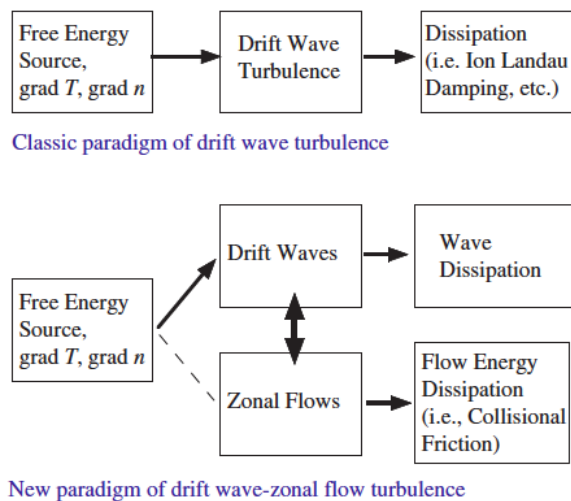
Figura 4.1: Archetype of dissipation pathways within turbulent framework[P H Diamond1 et. al.]

In order to describe the *modus operandi* of turbulent behavior, we are going to work in the framework of the Gyrokinetic description of the plasma. In this scheme, the fluctuations present in the parameters of interest can be analyzed in more detail, and it opens, also, a path for a reduced numerical solution of the whole process, which is interesting if one thinks about the use of computational resources as a tool for the description of the phenomena.

4.2 GYROKINETIC APPROACH

The gyrokinetic approach to the study of plasma dynamics allows us to describe perpendicular waves with $k_\perp \simeq \rho_{e,i}$, where $k_\perp$ is the typical wave number perpendicular to B, and $\rho_{e,i}$ is the

gyroradius. With time scales smaller than the ion cyclotron frequency. In order to compute any parameter, one needs first to compute the distribution function, as shown with the Vlasov theory.

From the Fokker-Planck equation, one must rewrite the main parameters in a perturbed expansion, which will be the focus of our analysis. The expanded equation is described as

$$\left[\frac{\partial}{\partial t} + v \cdot \nabla + \frac{q}{m}\left(v \times (B + B_p) + (E + E_p)\right) \cdot \frac{\partial}{\partial v}\right](f + f_p) = C[f + f_p] \tag{4.2}$$

In order to isolate the perturbed part, one could subtract from the previous equation an average of the same ensemble, leading to

$$\left[\frac{\partial}{\partial t} + v \cdot \nabla + \frac{q}{m}\left(v \times B + E\right) \cdot \frac{\partial}{\partial v}\right]f_p = \frac{q}{m}\left(v \times B_p + E_p\right) \cdot \frac{\partial(f + f_p)}{\partial v} - \Xi + C - \langle C \rangle_{average} \tag{4.3}$$

Here, it is important to notice that there is a crossed effect of the main value of the distribution function on the perturbed part of the main parameters, represented on the right hand side of the equation. The last term on the right hand side is an operator responsible for the description of the averaged out interaction between the fluctuations with the particles of the systems

$$\Xi = -\frac{q}{m}\left\langle (v \times B_p + E_p) \cdot \frac{\partial f_p}{\partial v}\right\rangle_{average} \tag{4.4}$$

One must, then, pass the frame of reference to the one coinciding with the guiding center of the particle's orbit. In this way, the dimensionality and complexity of the problem is reduced, since the complicated behavior of the particle around its guiding center can now be reduced to the movement of a parallel velocity, $v_\parallel$, and a magnetic momentum described as

$$\mu = \frac{mv_\perp{}^2}{2B} \tag{4.5}$$

A first order solution of equation 4.3, taking in consideration the gyrokinetic approach, is described as the adiabatic and non adiabatic solution of the perturbed distribution

$$f_{p,1}(r) = -\frac{q\phi_p(r)}{T} + H(r) \tag{4.6}$$

In terms of the gyrocenter position r, and as a function of the operator

$$h(r) = H(r) - \frac{q f_{p,0} \Im(r)}{T} \tag{4.7}$$

considering

$$\Im_p(r) = \langle \phi_p(r) - v \cdot A_p(r) \rangle_{average} \qquad (4.8)$$

The next order solution of the gyro-averaged equation is described as

$$\frac{\partial h}{\partial t} + (\hat{n}v_\parallel + v_d) \cdot \nabla H + v_p^d \cdot \nabla h - C[H] = -v_p^d \cdot \nabla f_0 \qquad (4.9)$$

Considering the perturbed drift velocity as $v_p^d = \hat{n} \times \nabla \Im_p / B$.

One could consider the filed to be described as

$$X_p(r) = X_*(r) e^{ik_\perp \cdot x} \qquad (4.10)$$

Considering $X_*(r)$, and $k_\perp$ to be slowly varying functions, we have the gyro average $\langle \cdot \rangle_{av}$ of the field perturbation as

$$\langle X_p \rangle_{av} = e^{ik_\perp \cdot x} X_* \left\langle e^{ik_\perp \cdot \rho} \right\rangle_{av} \qquad (4.11)$$

It could be described in terms of a Bessel function of first kind, considering

$$J_n(z) = \frac{1}{2\pi} \oint d\gamma\, e^{-in\gamma + iz\sin\gamma} \qquad (4.12)$$

we would have, therefore

$$\left\langle e^{ik_\perp \cdot \rho} \right\rangle_{av} = J_0(k_\perp \rho) \qquad (4.13)$$

$$\left\langle v_\perp e^{ik_\perp \cdot \rho} \right\rangle_{av} = iv_\perp J_1(k_\perp \rho) \frac{(k_\perp \times \hat{n})}{k_\perp} \qquad (4.14)$$

$$\left\langle \rho e^{ik_\perp \cdot \rho} \right\rangle_{av} = i\rho J_1(k_\perp \rho) \frac{\hat{n}k_\perp}{k_\perp} \qquad (4.15)$$

With a straightforward algebraic manipulation, we can describe the field $\Im_p$, as a function of the omitted gyrocenter frame of reference

$$\Im_p = J_0(k_\perp \rho) \left[\phi_p - v_\parallel A_{p,\perp} \right] + \frac{1}{2} \left[J_0(k_\perp \rho) + J_2(k_\perp \rho) \right] \frac{v_\perp^2}{w_c} B_{p,\parallel} \qquad (4.16)$$

Even when considered as a linear approach to the gyrokinetic theory, equation 4.9 has a complex solution, that makes it hard to be analytically solvable regardless of the simplicity of the

chosen geometry.

4.2.1 Ballooning properties

It is interesting to notice that, turbulence in plasma is normally elongated in the direction of the magnetic field, in the torus around the plasma bulk, but despite of that, a small perpendicular component exists. A way to analyze these short perturbations is to represent it in a flute-like description proportional to $e^{i(m\chi - n\phi)}$, being m, and n an integer number, and where χ is the poloidal, and ϕ is the toroidal coordinates.

Since the microinstabilities modes are not localized, but in fact spread over different flux surfaces, one could use instead of a flux approach, a ballooning representation, and compact the small perpendicular and elongated parallel modes. Disregarding the time dependence, and using a toroidal harmonic description of the perturbed fields X_p, we can have the expression in a compact form as (J. W. Connor, 1980)

$$X_p(r, \chi, \phi) = x_{p,n}(r, \chi)e^{-in[\phi - q(r)]\chi} \tag{4.17}$$

Considering, implicitly, a ballooning function depending on the poloidal angle χ.

Observe that, simple modes are radially periodic, and in order to simplify the approach, the constant parameters over the radial domain could be approximated, leading to a flattened profile, this is useful when $\rho \to 0$, and the perturbed parameters can be expanded in a perpendicular direction.

One could describe the non adiabatic part of the distribution h in a ballooning representation as (F. Romanelli, 1990)

$$\frac{v_\parallel}{qR}\partial_\theta h - i(w - w_D)h - C[h] = -i\frac{qf_0}{T}(w - w_T')\phi J_0(z) \tag{4.18}$$

With h, and ϕ as perturbed functions of the Ballooning function described above. Since the time derivatives are in function of the frequency, w_T is proportional to w', the diamagnetic frequency, and w_D is the magnetic drift frequency.

4.3 FLUX QUANTITIES

To understand how turbulence arises in the gyrokinetic theory, one could analyze the potential perturbation ϕ_p, corresponding to a perturbed drift velocity described as

$$v_p^d = \frac{\hat{n} \times \nabla \phi_p}{B}, \tag{4.19}$$

generating ambipolar effects. The average over a flux surface of this flow gives us the particle flux. Its dependence on the perturbed density n_p, and its direct relation to the potential perturbation are one of the indicators of its perturbed property.

Considering that $(\hat{n} \times \nabla \phi_p) \cdot r = i k_\theta \phi_p$, being r the unit vector in the radial direction, one could define the particle flux as

$$\Gamma = -\left\langle \frac{k_\theta T n}{qB} \left| \frac{q\phi_p}{T} \right|^2 \Re \left[\frac{n_p/n}{q\phi_p/T} \right] \right\rangle \tag{4.20}$$

Where the operator $\Re$ represents the density response of the plasma, and the whole left hand side is averaged in a flux surface. For a energy flux analysis, a similar operator to $\Re$ is responsible to represent the plasma temperature response

$$Q = -\left\langle \frac{k_\theta T^2 n}{qB} \left| \frac{q\phi_p}{T} \right|^2 \Re \left[\frac{T_p/T}{q\phi_p/T} \right] \right\rangle, \tag{4.21}$$

also averaged out over a flux surface. Notice that the perturbed properties of these quantities depend on the fact that the density, or temperature, perturbations are not aligned with the perturbed potential. If one thinks about the non adiabatic electron response, the particle flux is non existent if one does not consider any sort of impurities, and the adiabatic part of f_p does not lead to any flux in the radial direction, in this approximation.

Trivially, the magnitude of the fluxes depend directly on the perturbation potentials, and it is now easy to see the reason why this problem needs enormous computational resources in order to be accurately solved. In this cases, the best solution is the performance of nonlinear simulations, where the saturation mechanisms guides the magnitude of the perturbations.

Magnetic perturbations can, also, have an impact on the fluxes analysis. Following the gyrokinetic approach, the particle flux can be described as

$$\Gamma = \Re \left\langle \int d^3 v H \left\langle v_p^d \right\rangle \cdot r \right\rangle \tag{4.22}$$

Averaged over a flux surface. Here, H is determined by the electrostatic gyrokinetic equation and $\left\langle v_p^d \right\rangle = \hat{n} \times \left\langle \phi_p \right\rangle / B$. The electromagnetic case has H represented by 4.9 with source terms from other origins such as $\left\langle v_p^d \right\rangle = \hat{n} \times \Im_p / B$.

4.4 ONSET OF MICROINSTABILITIES

Microinstabilities are thought to be a good candidate to solve the problem of anomalous transport. Given the fact that microturbulences have wave lengths comparable with the ion gyroradius, and considering that an overall picture of turbulent transport could help us to have hints in threshold saturation levels and parametric dependence of fluxes, one could possibly identified driven mechanisms with the help of a more detailed analysis.

Instabilities transfer the free energy from the plasma to turbulent flows. Drift waves are a particular class of waves that exist as a source of plasma turbulence. Depending on the kinetic pressure normalized to the magnetic pressure $\beta = p/(B^2/2\mu_0)$, electromagnetic or electrostatic instabilities may be predominant. For plasmas near the Maxwellian distribution, the growth rate of instabilities is approximated by $((T_e + T_i)^{1/2}/m_i)/a$, where a is the plasma radius.

For low values of β, or large magnetic field, the B constrains the motion of the plasma and, therefore, the resulting turbulence is electrostatic. In contrast to the case of high β, where a fluid-like behavior is seen, and turbulence arises in the form of Alfven waves.

Microturbulence led by microinstabilities are, normally, of the order of the gyro-Bohm diffusion rate, $D = \rho^2 C_s/a$, where C_s is the plasma sound speed, with relatively small amplitudes. In this section, we are going to deal with three prominent microinstabilities, Ion and Electron Temperature Gradient, ITG and ETG, respectively, and Trapped Electron Mode (TEM). It is important to notice that, due to its dimensional size, and its propagating velocity, microinstabilities does not perturb the plasma quasineutrality approach. Notwithstanding the importance of all three parties, a greater attention will be given to the ITG mode.

4.4.1 Ion Temperature Gradient

In order to analyze the ion response, one could consider a energy-dependent Krook collisional model in a strong ballooning limit

$$C[h] = -\frac{\nu}{x^3}h \tag{4.23}$$

and after some algebraic manipulation, one gets

$$h = \frac{qf_0}{T} \frac{w - w'[1 - (\frac{3}{2} - x^2)\eta]}{w - k_\parallel v_\parallel - w_D^*(\frac{x_\perp^2}{2} + x_\parallel^2) + \frac{i\nu}{x^3}} J_0(z)\phi \tag{4.24}$$

Some considerations must be taken into account here. The parallel comprehensibility is described by $k_\parallel v_\parallel$, and $x = v/v_T$, and $\eta = L_n/L_T$. Here, w_D^* is described as

$$w_D^* = \frac{w_D v_T^2}{v_\perp^2/2 + v_\parallel^2} \tag{4.25}$$

Remembering that w_D is the magnetic drift frequency. In 4.24, transforming the ion density response from gyrocenter space to real space, lead us to a velocity integral, one in which the poles are responsible for the interpretation of resonances and destabilizing modes. Depending whether we have a magnetic drift or a collisional resonance mode, the ITG is be defined as slab or toroidal.

If one considers a full dispersion relation, with electrons in the response term, the resultant differential equation would be hardly possible to be solved analytically without further considerations.

The ITG is considered a passing particle mode with a frequency range between the ion and electron. For an adiabatic electron response, equation 4.24 holds as a first approximation. In a toroidal geometry, the curvature becomes the main driving mechanism. The quasineutrality leads us to an eigenfuction problem, and the solution peaks at the ballooning angle equals to 0, in the region where the curvature is considered not weak. The result is a ballooning structure, where the magnetic drift destabilize the mode through ITG.

Figure 4.2 help us to illustrate the *modus operandi* of the mechanism. There, we can observe how the temperature perturbation in the plasma, in the outer part of the torus, is affected by the magnetic drift of the particles, leading to a growing density perturbation. The density perturbation generate, then, $E \times B$ flows. It is easy to see that the curvature of the torus generate good and bad regions on the plasma, that will directly affect the stabilization of the ITG modes. The ballooning form is gained due to the drive source and the stabilization shape's dependence on the poloidal angle.

Observe that turbulent fluctuations generate no toroidal nor poloidal mode perturbations, and are therefore not dumped by Landau mechanisms. The generated flows appear to be mostly in a poloidal direction inside each of the flux surfaces with a direction varying on a radial scale.

The in-flux-surface zonal flow, together with neoclassical flows, possess a strong stabilizing effect, that when considered with the radial correlation length, can lead to a reduction in the transport level.
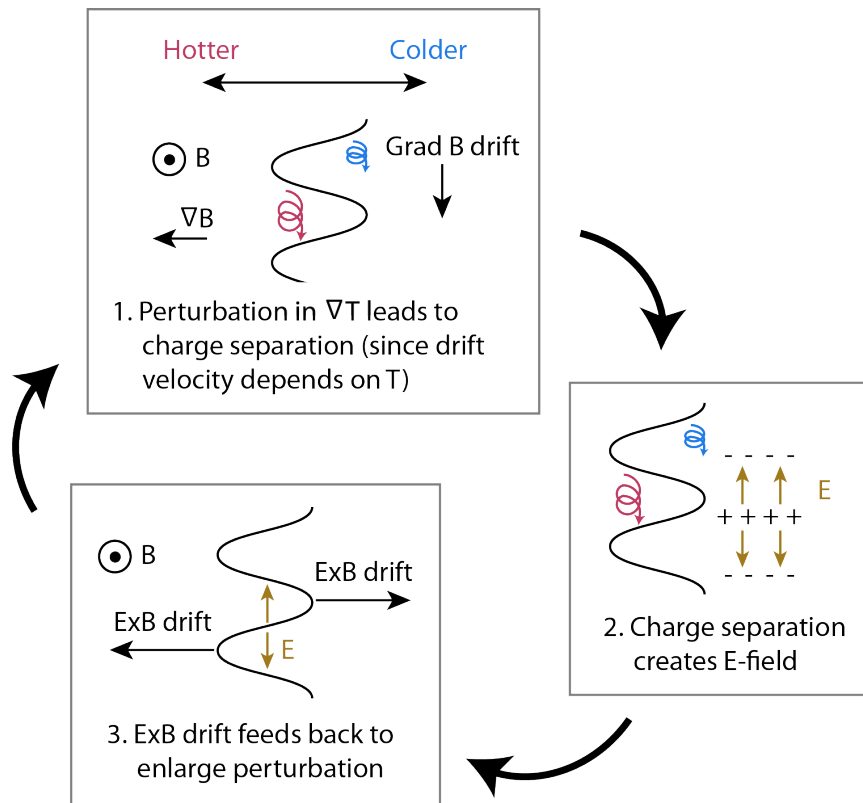
Figura 4.2: ITG instability[credit:Aaron Scheinberg]

4.4.2 Electron Temperature Gradient

Considering Ions responding adiabatically, but electrons not, a microinstability mode can arise in the form of the ETG mode. Because the ions respond adiabatically, they are free to cross the field lines in response to changes in the potential, disregarding zonal flows, since the ion response is to the full variation in the electric potential.

The extend of the radial scale of the constant potential contours is limited by the ion gyroradius, that way, the ions are free to respond adiabatically. Due to a great anisotropy, the ETG transport can be comparable to the ITG with zonal flows (F. Jenko, 2000) . In the electrostatic and adiabatic limit, the ETG mode is similar to the ITG mode, with the ions interchanged by the electrons.

Recently, it was argued that gradient driven turbulent modes are nonlinearly generated by radially extended non linear perturbations, called streamers (J. Drake, 1988). An analysis of this phenomena shows us that theses streamers saturate by the secondary Kelvin-Helmholtz instability mechanism.

ETG structures are possibly dominated by radially extended streamers, generated from a isotropic turbulent state within a modulational instability mechanism. From the Braginskii 2- fuid

equations a model for the ETG mode in the hydrodynamic approximation can be drawn. Consisting of the electron continuity equation, the parallel equation of motion and the temperature equation coupled with expressions for perpendicular drifts of the electron fluid, we have the following equation

$$v_{e,\perp} = -\frac{c}{B^2} B \times \left(E + \frac{\nabla p_e}{qn} \right) \left(1 - \frac{B_{p,\parallel}}{B} \right) - \frac{c}{Bw_e} \left(\frac{d}{dt} + v_* \cdot \nabla \right) E_\perp + v_\parallel \frac{B_{p,\perp}}{B} \qquad (4.26)$$

Where we can observe a $E \times B$ drift, together with diamagnetic and polarization drifts. Note that the perturbation of the magnetic field in the parallel direction, $B_{p,\parallel}$ affects the equation in more than one term, and therefore, couples the ETG mode to the perpendicular and parallel magnetic perturbations directions. The streamers are, then, nonlinearly excited through modulation instability, arising from scaling transformations. Nonlinearities arising from the electrostatic perturbed equations manifest themselves and large amplitude anisotropic eddies are created, such eddies represent the streamers discussed in this paragraph. A modulation instability analysis indicates that homogeneous isotropic turbulence of ETG modes is unstable to the formation of streamers.
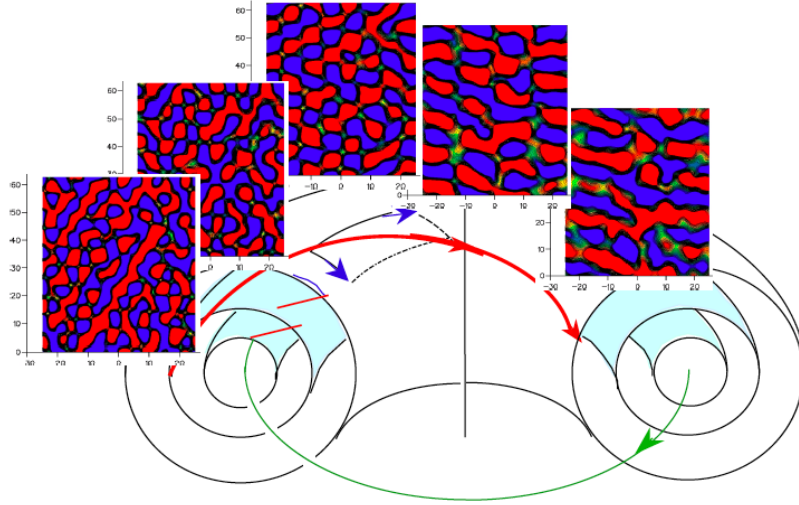

Figura 4.3: ETG saturation and streamers formation[credit:20th IAEA Fusion Energy Conference]

In figure 4.3 we can easily observe how streamers are formed close to the good curvature in the torus, where the shear is higher, holding up the argument that magnetic shear could possible be responsible for turbulence anisotropy.

4.4.3 Trapped Electron Mode

Trapped Electron Mode (TEM) appears when non adiabatic trapped electron response is introduced, generating a new root, distinct from the ITG mode. In this case, trapped electron bounce

between the High Side Field and the Low Side Field like small magnetic dipoles, μ, due to the magnetic mirror force generated between the inside and the outside region of the torus. These electron are mostly found in the unfavorable part of the curvature, giving a direction to the curvature drift, and the local electrostatic field $E \times B$ gives origin to microinstabilities that, due to its inertia, does not follow the electrostatic perturbation and behave, therefore, non-adiabatically.
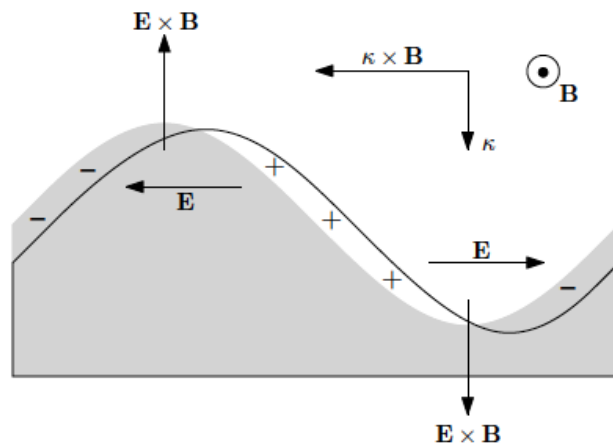

Figura 4.4: Trapped particle mode instability[credit:Ben Dudson]

Collision plays an important role in the rise of trapped instabilities, since if they are not too frequent, these particle can remain longer in the bouncing regime. Trapped electron mode is a prominent contributor of the anomalous fluxes in tokamaks, and the study of electron cyclotron heated Ohmic plasmas demonstrate us the importance of trapped electron mode driven transport.

TEM are similar to sausage instabilities, in the sense that, as seen in figure 4.4, a charge separation is formed due to the bouncing of electrons. Note that, due to the nature of the effect of the passing particles, they act as a background and with Boltzmann response.

4.5 OVERVIEW

It was shown in this chapter the role of microturbulence in order to quantify the turbulent transport, and the onset of three modes of microinstabilities. Ion Temperature Gradient, Electron Temperature Gradient, and Trapped Electron Mode, are found to be in a fairly adjacent range of proximity.

The different growth rates, γ, of these instabilities is observed in figure 4.5. It is easy to un-
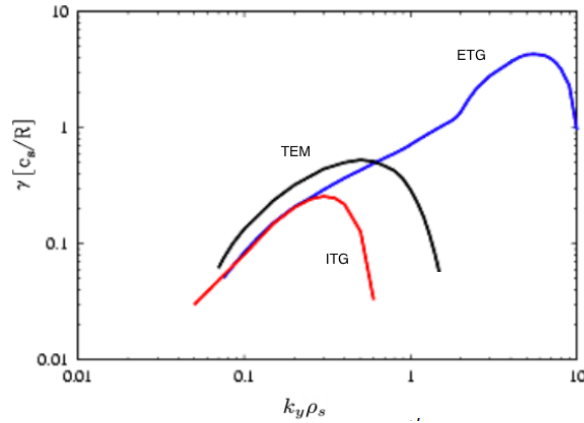
Figura 4.5: Range of instability growth rate, γ, for different microninstabilities range [credit:F. Jenko]

derstand this image when one has in mind the scales of the microinstabilities *per se*, being ion larmor radius for ITG, electron larmor radius for ETG and in-between for TEM.

We saw also that, zonal flows generated by microturbulences are sheared, disrupting its eddies, decreasing thus transport levels, which could indicate a stabilization mechanism arising from the initial considerations. In that panorama, the shearing of $E \times B$ flows could generate a mechanism responsible for the reduction of the anomalous transport (B. N. Rogers, 2007).

One could reasonably argue that anomalous transport can, in fact, be described by turbulent transport. Most specifically, one could claim that the nonlinear dynamic of microturbulence generated by small scales structures could give us a valid picture of tokamak transport. In order to do so, computational validations must be done is the aim of our next chapter.

5 NUMERICAL SIMULATIONS

In the previous chapter, we learnt that the once valid transport theory fails to predict the correct flux levels of real experiments. We, then, rapidly discussed an approach on the framework of gyrokinetic theory, in order to model which phenomena may be taking place instead of exclusively the neoclassic transport.

We discovered that microinstabilities may be the mechanism responsible for driving free energy flows from different scales in the plasma, and therefore, they could be a possible explanation for the flux levels observations, and why they are not met when only neoclassic transport theory is considered.

In order to validate the gyrokinetic theory, numerical simulations can be performed, and realistic fluxes levels are computationally predicted. In this chapter, we are going to talk about one of the numerous codes used to solve the problem of the anomalous transport, but before deepening ourselves on the idiosyncrasies of specific codes, and in order to understand the cpmplexity of the problem of turbulence, a few words will be given in an important topic, High Performance Computing.

5.1 HIGH PERFORMANCE COMPUTING

High Performance Computing (HPC) is defined (G. Sravanthi, 2014) as "*the practice of aggregating computing power in a way that delivers much higher performance than one could get out of a typical desktop computer or workstation in order to solve large problems in science, engineering, or business*".

Following the advent of the new era, where computers are used as an indispensable assessment tool in research and development, some computing demanding problems cannot be approached with only one processor, due to its high complexity and nonlinearity properties, and a cluster of computers is needed. In this cases, a program is said to be "parallelized"when its code lines are adapted to run in a parallel processing environment, like a supercomputer.

Problems involving turbulent flows are among the most used in high performance computing environments, like in the case of turbulent transport in thermonuclear plasmas, as studied in the present work.

5.1.1 Parallelization

Parallel computing is a form of computation in which different parts of the code are processed simultaneously. A traditional computer code is normally written in a linear sequence of tasks, and these processes are computed in the order described by the code. The parallel paradigm allows us to process different executions at the same time, by dividing the workload in smaller parts, dividing them among the working nodes, and communicating different processors between themselves in order to maintain the hierarchic properties of the computed data. In the software point of view, two important levels of parallelism deserve our consideration, data parallelism and task parallelism.

The data parallelism divide the data and distribute it among the working nodes, it is the most used form of parallelism in Particle In Cell programs. Task parallelism relies on the identification of the different tasks, and the description of the software in a way that allows independent tasks to run simultaneously, in different processors.

In the hardware level, other form of parallelizations are worth our attention. We are going to briefly discuss two of them in the following chapter.

5.1.1.1 Single-instruction-multiple-data

In data parallelism, single-instruction-multiple-data (SIMD) codes can be parallelized by distributing the data across the different nodes in the system. In this scenario, the data must have an hierarchy such that it allows the parallelization without any loss of performance and accuracy. The method can be applied in arrays and matrices, where the data is processed simultaneously.

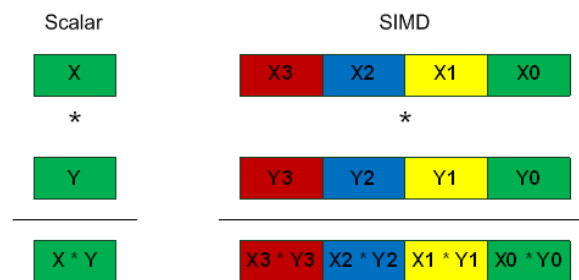Figura 5.1: Data parallelism scheme for SIMD architecture. [credit: Intel]

In image 5.1 we can see how the data, X and Y variables, can be computed in a system with four processors (indicated with the different colors) at the same time, without loss of correctness of the result. This process allows to a optimum load balance of the tasks and a synchronous computation, where all processes are synchronized at regular points.

5.1.1.2 Multiple-instruction-multiple-data

Multiple-instruction-multiple-data, (MIMD), is an approach in which the tasks are divided into different threads and processed at the same time. The parallelization occurs when different threads are executed on the same or different data. In general, the threads must communicate with each other in order to allow the data to be shared among the nodes when there is need for data sharing among the threads.

In the most general case, MIMD codes allow for the simultaneous computation of multiple autonomous processors executing different instructions on different data. This allows for a high performance computation of the data, with less waste of computational resources by idle processors.
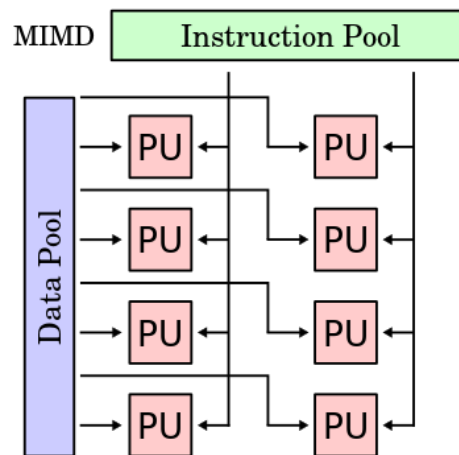

Figura 5.2: Data parallelism scheme for MIMD architecture. [credit: Colin M.L. Burnett]

In image 5.2 we can observe how the MIMD architecture works in processors level. The Instruction pool is divided and distributed to the processing units (PU), where each PU is responsible for a fraction of the total data pool.

5.1.2 Message Passing and Open Multi-Processing

The message passing is a technique used to communicate different processes. It provides a layer for common services to communicate a systems made up of sub-systems that can be invoked in different locations and at different times. Open Multi-Processing serves as thread manager, allocating the proper resources for each invoked thread, and ensuring that the message is put in a queue if the desired object is not currently available, and then invoking the message when the object is accessible. Two kinds of approaches are discussed here, Message Passing Interface (MPI) and Open Multi-Processing (OpenMP).

MPI is a message passing protocol used for communication in parallel systems. It is defined as (L. Gropp, 1996) "*It is a message-passing application programmer interface, together with protocol and semantic specifications for how its features must behave in any implementation.*". It allows for the inter node communication among the processes, using a communication network, as seen in image 5.3.
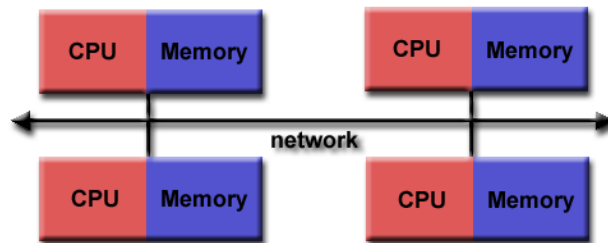

Figura 5.3: Distributed shared memory scheme. [credit: Blaise Barney]

OpenMP is an Application Program Interface (API), or a set of protocols and tools used for the development of software applications, and it is used to direct multi-threaded, shared memory parallelism. It uses a Fork-Join mechanism, as seen in image 5.4, in which a thread, labeled 'master', invoke parallel threads in order to realize a task.
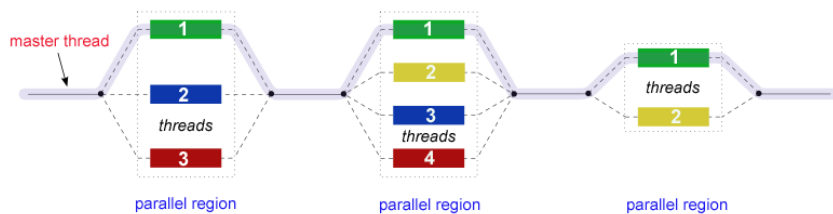

Figura 5.4: OpenMP Fork-Joint mechanism. credit: Blaise Barney

As it can be seen in the image, after the task is completed, the master thread is responsible for synchronize and terminate all the team threads, and the information executed by them is made available for the next step of the computation.

5.1.3 Executing in parallel

Different from an ordinary computer, when a simulation is started in a supercomputer, the job, as it is called in the HPC jargon, is submitted to a batch queue. The queue system is responsible to schedule the requested number of processors and check the availability of the processors in the system. The administrator is also responsible for the verification of the job priority, and for the supervision of idle processors in the system. The job queue system is a useful tool when

one wishes to have a optimum utilization of a large number of computational resources. The job queue is useful to have a common policy for several users and assign fairly the execution time for their jobs.

As it can be seen in image 5.5, the job is submitted to the system through the login nodes, or heads. The job is scheduled and put in wait until the queue system allows the code to run. The simulation is, then, performed in the various computer nodes available in the system.
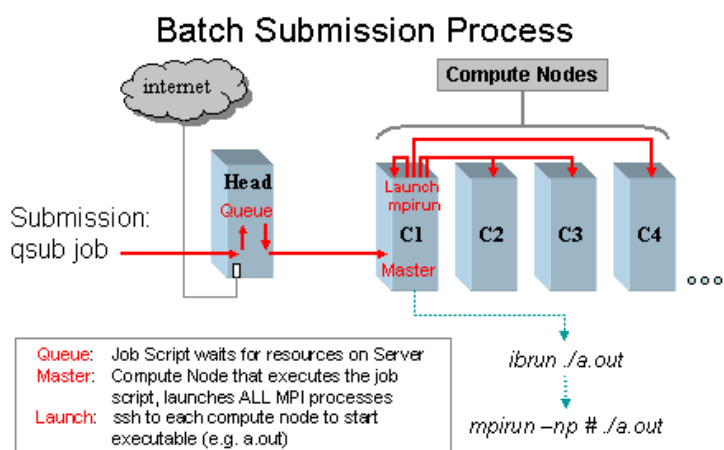

Figura 5.5: Scheme of a submission process. [credit: Brandon Barker]

It is important to keep in mind that not every program is suitable to be optimally used in an environment like the one described above. In order to be properly used, the code should be parallelized.

All this information gives us enough background to comprehend better one of the innumerous approaches used to solve the anomalous transport problem. The code described in the following section runs in a hybrid MPI-OpenMP environment, and has a linear scalability up to 250.000 processors.

5.2 THE GENE CODE

The GENE, acronym for Gyrokinetic Electromagnetic Numerical Experiment, is an "*open source plasma microturbulence code which can be used to efficiently compute gyroradius-scale fluctuations and the resulting transport coefficients in magnetized fusion and astrophysical plasmas. To this aim, it solves the nonlinear gyrokinetic equations on a fixed grid in five-dimensional phase space (plus time)*". The code solves the equations in a flux-tube domain, and a solver for the neoclassical equilibrium is already considered in it. The GENE code is highly parallelized,

and it runs on most of the world's powerful supercomputers.

As we have seen, fast gyromotion can be analytically removed from the initial equations, and therefore, separately computed. In GENE, the objects of interest are the time-dependent distribution function in a five-dimensional phase space of electrons, the main ion, and other particle species, apart of the Maxwell field equations. Remembering that now, due to the gyrokinetic approach, the helical movement around the field lines is reduce to a linear movement of a magnetic dipole.

It is considered that in the flux-tube approximation, as seen in the left hand side of image 5.6, the neoclassical equilibrium contained in the gyrokinetic equations decouples as a non-fluctuating part, and then both parts can be solved separately. The code considers magnetic fluctuations in perpendicular and parallel directions, individual Landau-Boltzmann operator collision discretized in a finite volume scheme for each of the particle species, and a general MHD equilibria, where local Miller, consistent circular and other models are considered.
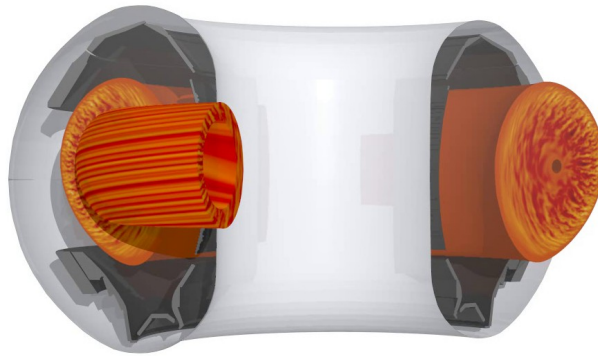

Figura 5.6: Global GENE simulation of AUG reactor. credit: genecode.org

The operator is discretized in all direction, being the x, and y direction spectrally discretized. The perpendicular directions are treated with a careful method involving a special kind of Fast Fourier Transform (FFT) algorithm solver, due to its term involving $E \times B$ nonlinearities. The parallel direction is discretized using n_z points in the poloidal angle, and a trapezoid rule is used in order to integrate the terms and compute the volume averages.

At this point, it is interesting to recapitulate the last topic, in which HPC was discussed. In order to solve the eigenvalue spectrum of the linear gyrokinetic operators, GENE uses a extension called SLEPc, from the PETSc package, in which, in order to solve the eigenvalue problems, it repeatedly applies matrix-vector multiplications representing the evaluation of the linearized gyrokinetic equation. In a non HPC environment, such processes, for a large group of particles would take up to a decade for a linear run. Because the matrix problem can be properly distributed in the different nodes, the computing time is reduced to days.

An initial problem case is also possible to be done in GENE, the eigenvalue solver is in this case the discretization of the time derivative of the linearized gyrokinetic equation, and computation of the initial value problem, with a superposition of the linear modes as initial conditions. By using an appropriate step scheme, the initial solver is normally faster than the eigenvalue solver, in GENE, up to the time of this writing, a modified Runge-Kutta of 4th order is normally used as a time discretization method.

For non linear simulations, the capability to run in many processors at the same time is essential in order to have the results of the simulation within a life-time period. A typical non-linear simulation of gene, with a $nx0$ box size equals to 256, and L_x equals to 128, and with $128 \times 64 \times 24 \times 48 \times 8 \times 2$ points for the distribution function of the main parameters (k_y, z, $v_\parallel$, μ and species), would take up to 100.000 CPU-hours to run a complete simulation.

GENE run in a distributed and shared memory architecture. In the distributed case, a heavy use of MPI is required. In these cases, all the parameters of interest, including the field equations and the elements of the Runge-Kutta schemes are cut into sub-arrays and distributed to the processors. In the case that a processor needs the information from a parameter in another processor, to compute, *e. g.* spatial derivatives, the information has to be sent explicitly from one processor to the other, by using the MPI standards. GENE is MPI-parallelized along the k_y, z, $v_\parallel$, μ and species directions.

Because it is also parallelized within its numerically expensive loops, the use of OpenMP, allows for efficient use even when MPI parallelization is not possible. The most recommended use of the code is in hybrid mode, MPI/OpenMP, in which the performance is enhanced up to 300.000 folds.

5.2.1   The equations

An equation of interest solved in the GENE code is the Gyrokinetic Vlasov equation for the different species. Taking in consideration the collision operator, consisting of advective and diffusive terms in the velocity space, we have

$$\frac{\partial f}{\partial t} + \dot{X} \cdot \nabla f + \dot{v}_\parallel \frac{\partial f}{\partial v_\parallel} + \dot{\mu} \frac{\partial f}{\partial \mu} = C(f) \tag{5.1}$$

where f represents the distribution function of a given species. It must be taken in consideration that $\dot{\mu} = 0$, and that here, the term $\dot{X}$ represents the gyrocenter position, and is described

as

$$\dot{X} = v_\parallel \hat{n}_0 + \frac{B_0}{B_{0,\parallel}} v_\perp \tag{5.2}$$

The drift velocities must also be taken care of. GENE combines them in one single equation, creating a dependence with a generalized potential

$$v_\perp \equiv \frac{c}{B_0^2} \chi \times B_0 + \frac{\mu}{m\Omega} \hat{n}_0 \times \nabla B_0 + \frac{v_\parallel^2}{\Omega} (\nabla \times \hat{n})_\perp \tag{5.3}$$

And considering the generalized potential as

$$\chi = \overline{\phi}_1 - \frac{v_\parallel}{c} \overline{A}_1 + \frac{\mu}{q} \overline{B}_{1,\parallel} \tag{5.4}$$

The parallel velocity is another parameter needed in order to compute the energy and fluxes in different direction. Considering the electric field described as

$$E_1 = -\nabla \phi_1 - \frac{\hat{n}_0}{c} \frac{\partial}{\partial t} A_{1,\parallel} \tag{5.5}$$

The parallel velocity is computed as

$$\dot{v}_\parallel = \frac{\dot{X}}{mv_\parallel} \cdot (q\overline{E}_1 - \mu \nabla (B_0 + B_{1,\parallel})) \tag{5.6}$$

In equation 5.6, it is important to notice the dipole momentum connection with both the initial and parallel perturbed magnetic fields.

In order to solve the problem, Ampere's law and the Poisson equation needs to be, also, implemented in the gyrokinetic framework:

$$\nabla_\perp^2 \phi_1 = -4\pi \sum qn_1 \tag{5.7}$$

In which n_1 is related to the density perturbation, and

$$\nabla_\perp^2 A_{1,\parallel} = -\frac{4\pi}{c} \sum j_{1,\parallel} \tag{5.8}$$

$$B_{1,\parallel} = -4\pi \sum \frac{p_{1,\perp}}{B_0} \tag{5.9}$$

Where the current perturbation, j_1, is summed over all the species.

In a local approximation, the moments can be described in a Fourier space as

$$n_{1,k} = \frac{2\pi B_0}{m} \int dv_\parallel d\mu \left[J_0 h_{1,k} - q\phi_{1,k}\frac{F_0}{T_0} \right] \qquad (5.10)$$

$$j_{1,\parallel,k} = q\frac{2\pi B_0}{m} \int dv_\parallel d\mu v_\parallel \left[J_0 h_{1,k} - q\phi_{1,k}\frac{F_0}{T_0} \right] \qquad (5.11)$$

And,

$$p_{1,\perp,k} \equiv \frac{2\pi B_0}{m} \int dv_\parallel d\mu \mu B_0 I_1 h_{1,k} \qquad (5.12)$$

Considering the non adiabatic part of f_1 as

$$h_1 \equiv f_1 + \left[q J_0 \phi_1 + \mu I_1 B_{1\parallel} \right] \frac{F_0}{T_0} \qquad (5.13)$$

It is necessary to recall that h_1 must be computed for each one of the species considered in the problem. The Bessel function is given by

$$J_0 = J_0(k_\perp \rho) \qquad (5.14)$$

And,

$$I_1 = I_1(k_\perp \rho) = 2\frac{J_1(k_\perp \rho)}{k_\perp \rho} \qquad (5.15)$$

5.2.2 The output files

After the simulation is finished, GENE has a large number of output files written in the desired directory. The main output files are the "nrg", containing time trace information such as density and temperature, the files "field"and "mom"have three-dimensional information about the fields and moments of the distribution function, written in smaller time steps than the "nrg"files due to its sizes.

In the "nrg"file, the normalized fluctuating quantities are spatially averaged with respect to the full simulation volume. Considering f^{pc} the particle distribution function, the heat and parallel momentum fluxes are computed as

$$\Gamma = \int d^3 v f_1^{pc} v_D \tag{5.16}$$

$$Q = \int d^3 v (\frac{1}{2} m v^2) f_1^{pc} v_D \tag{5.17}$$

$$\Pi = \int d^3 v (m v_\parallel) f_1^{pc} v_D \tag{5.18}$$

Where v_D is the generalized $E \times B$ velocity drift. The fluxes are divided into an electromagnetic and electrostatic radially projected components.

The "field"file is a binary file, consisting of the time steps and complex values in three dimensions (k_x, k_y, z).

$$\phi_1 \left\{ A_{1\parallel} \left[B_{1\parallel} \right] \right\} \tag{5.19}$$

Being $A_{1\parallel}$ and $B_{1\parallel}$ only computed in the electromagnetic case.

The "mom"file contain values for each of the computed species, and it consists of velocity space moments, in which their average combination yield the parallel heat current density

$$q_{1\parallel} + 1.5 p_0 u_{1\parallel} = \frac{1}{2} \int d^3 v v_\parallel^3 f^{pc} \tag{5.20}$$

$$q_{1\perp} + p_0 u_{1\parallel} = \frac{1}{2} \int d^3 v v_\parallel v_\perp^2 f^{pc} \tag{5.21}$$

Where $u_{1\parallel}$ is defined as

$$u_{1\parallel} = \frac{1}{n_0} \int d^3 v v_\parallel f_1^{pc} \tag{5.22}$$

As outputs, GENE still has other files, manly involving neoclassical results, information about the velocity space, information about instabilities growth rates γ and frequencies ω, checkpoint files, and information about the time evolution of free energy quantities.

Considering the modified perturbed distribution function

$$h_1 = F_1 + \left(\frac{q}{T_0 \overline{\phi}_1} + \mu B_{1\parallel} \right) F_0 \tag{5.23}$$

58

The free energy operator is described as a volume average

$$\varepsilon[A] = \sum Re \left\{ \left\langle n_0 T_0 \int d\mu dv_\parallel \frac{h}{F_0} A \right\rangle \right\} \qquad (5.24)$$

Taking into account the summation over all species, n_0 as the equilibrium density, T_0 the equilibrium temperature, and considering A to be correspondent to the distribution function F_1 or any of its time derivatives in the gyrokinetic equation, and normalized to units of reference.

5.2.3 The Diagnostic Tool

GENE has an state-of-the-art diagnostic tool. It uses an IDL environment, and assists the user to easily navigate through the data, showing parameters of interest in different time steps of the simulation, if required.

One could, following the scope and objective of the present work, analyze the different instabilities growth rates for different scenarios, and thus, evaluate the impact of modifications of the set up of experiments. In our case, it would be interesting to study the effective particle and heat flux levels, and study the effectiveness of the gyrokinetic approach in order to give support to the anomalous transport problem.

The Graphical User Interface, (GUI), allows for a visualization of all the parameters of the simulation, as well as a pre-vizualization of some of the required outputs in a preview window offered in the GUI itself. The data can be treated within the tool, and a careful selection of final outputs give us the possibility to select specific variables to be analyzed.

The next chapter will give us a clearer picture of the functionalities of the GENE diagnostic tool, as well as display some of its idiosyncrasies.

5.3 SUMMARY

In this chapter, we studied a particular numerical solver of the turbulent transport problem, the GENE code. We consider some of its eigenvalues solver, and the importance of HPC in solving problems of this magnitude.

We identified the equations used in GENE, and it can be observed that it is in agreement with

the theory described in the past chapters, giving us the possibility to argue in favor of the accuracy of the implementation of the problem.

We then examined the files produced from a simulation, and since one wants to demonstrate the effectiveness of the gyrokinetic approach, our object of interest will be the fluxes and, to analyze the impact of microturbulence in the energy flow, the instability growth rate.

In the previous chapters, we have studied how the transport in the plasma is understood from a classical and neoclassical point of view. We have, then, studied the turbulent approach to solve the problem of higher-than-expected flux levels that appeared when experimental results were contrasted with the theoretical values.

In this conjuncture, the studied gyrokinetic approach is the framework in which turbulent transport can be simplified from a 6 dimensional phase-space, plus time, to a 5 dimensional phase-space, plus time. In this approach, one can, additionally, investigate the onset of microinstabilities, a phenomena that is thought to be the mechanism in which the energy is released from the different-sized scales in the turbulent motion of the plasma.

This approximation brings us, together with the assistance of high performance computing, to the description of a gyrokinetic code capable of solving numerically gyrokinetic set of equations for a realistic case, enabling us to contrast theoretical levels with experimental ones. The purpose of this chapter is to recognize and understand the accuracy of the gyrokinetic model based on the literature. More precisely, a throughout analysis of the literature is done in order to define the level of efficiency of the gyrokinetic approach, using the code GENE as reference.

6.1 SELF ORGANIZED CRITICALITY

Self organized criticality (SOC) is a phenomena exhibited by dynamical systems with spatial degrees of freedom. It is a mechanism that develops local instabilities and relaxes them. Scale invariance and self-similarity are features of self organized systems.

In magnetically confined plasmas, specifically in toroidal confinement, SOC is thought to play a role in the formation of the H-modes in tokamak plasmas. H-modes are states in which the confinement time of the plasma is enhanced by a factor of 2 or more. It is still unknown which exact mechanism triggers the formation of H-modes. In this state, the formation of an Edge Transport Barrier (ETB) is seen to appear in the pedestal of the plasma. The rapid rise in the pressure profile due to the reduction of transport through the ETB is responsible for the enhancement of the confinement.

As seen in image 6.1 the formation of a more augmented profile is seen with the appearance of the Internal Transport Barrier (ITB). This advanced scenario is being currently explored.
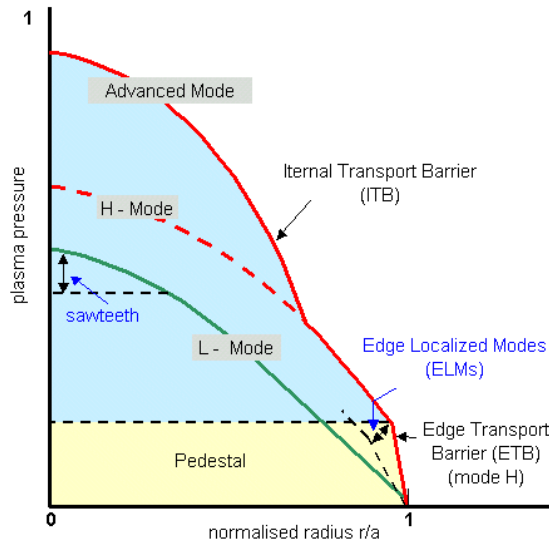
Figura 6.1: Formation of enhanced modes in a tokamak scenario [credit: CEA]

Although it is known that the formation of ITB and ETB are responsible for the enhancement of the confinement, no known mechanism describes precisely the formation of the barriers. In this sense, a broad group of possible ways all include features of a SOC systems.

A study (M. Mavridis *et al.*, 2014) determines that some features of SOC can be described with the gyrokinetic code GENE. The use of local gyrokinetic simulations has been already proposed to the study SOC systems by McMillian *et al* as well.

The study of time series of GENE radially averaged heat fluxes marginally stable give us insights in some SOC properties that arise from the gyrokinetic system of equations. In this cases, the contrast of the gyrocentered approach with known expected physical mechanism reassure the validity of this framework.

An important property of SOC systems is the $1/f$ noise, which is a low-frequency spectra with a power-law behavior $f^{-\beta}$, observed in different time scales. It is described in the statement from Per Bak *et al.*, 1987.

"The system will become stable precisely at the point when the network of minimally stable states has been broken down to the level where the noise signal cannot be communicated through infinite distances. At this point, there will be no length scale in the problem so that one might expect the formation of a scale-invariant structure of minimally stable states."

We could try to imagine a sandpile with a large slope. The collapse of such pile stops when a critical value is reached and the system is stable with respect to small perturbations. In this example, the $1/f$ noise is the "dynamical response of the sandpile to small random perturbations".

A power spectrum of time series analysis of the GENE data is a convenient tool to analyze the noise property in the gyrokinetic equations.
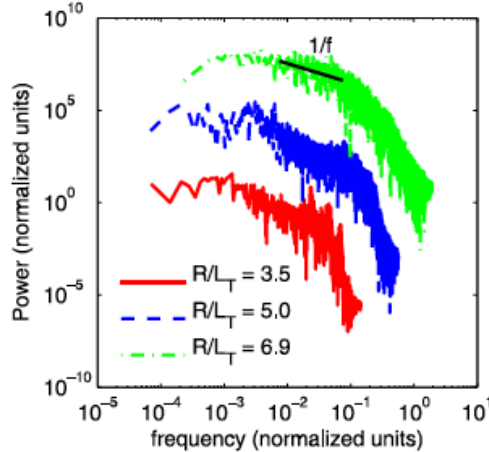

Figura 6.2: The $f^{-\beta}$ behavior observed in a power spectra of GENE simulation [credit: M Mavridis]

We can observe in figure 6.2 that for different regions of the frequency range, the β exponent of the power-law decay is different. Intermediated frequencies represent the overlapping of avalanches, a common feature of SOC systems, and a phenomena similar to streamers, discussed in the present work. The last region of higher frequencies is associated with small scale events.

In figure 6.2, the colors red, blue and green represent different simulations with distinct temperature gradients L/R_T, we can see that as the temperature gradient changes, the position of the $1/f$ behavior changes as well. This behavior can be interpreted in terms of the number of k_y modes in the Fourier space for the various parameters.

Regarding the avalanche effects, a main feature in a SOC system, statistic analysis of the heat flux can be performed in order to establish their features and properties in a radius time plane.

The formation of radial traveling two-dimensional structures in the contour plot of the heat flux, associated with tilting reinforce the idea that SOC peculiarities known as avalanches are also found in non linear GENE simulations. The large radial extend of such structures is a common attribute of avalanche processes.

The analysis of the fractal dimension is an important assessment tool, it is a ratio that provide
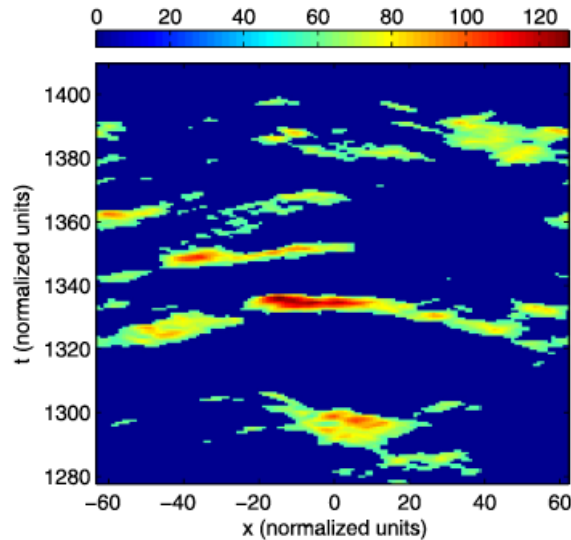
Figura 6.3: Heat flux fluctuations in normalized scales for a $R/L_T = 6.5$ [credit: M Mavridis]

a statistical indicator of complexity. It compares the resolution in a fractal pattern, and how it changes with the scale at which it is measured. From figure 6.3, the calculation of the probability distribution function of the radial extends, computed from the determination of the extend of these structures in the radial direction, together with the fractal dimension analysis, allows us to identify the structure in figure 6.3 as an avalanche.

6.2 SHORTFALL

The evolution of the numerical solutions of turbulent transport in the gyrokinetic framework has seen a substantial improvement in the last decades, either due to the refinement in the gyrokinetic theory, or due to the rump up in the use of high performance computing.

In 2008, an analysis (C. Holland *et al.*, 2008) done with the support of another gyrokinetic tool known as GYRO, in a L-mode discharge from the DIII-D tokamak, from General Atomics, showed an underprediction of a factor of seven of the energy flows, and by a factor of 3 of the fluctuation amplitudes in the outer layer of the tokamak, the ion heat flux mismatch can be seen in figure 6.4.

The significant discrepancy between the experimental and computed heat flux is known as *shortfall*. Questions related to the universality of the shortfall in L-mode and the extent of the gap from the simulation and the experimental values put into question the validity of the physics underlying the gyrokinetic approach.
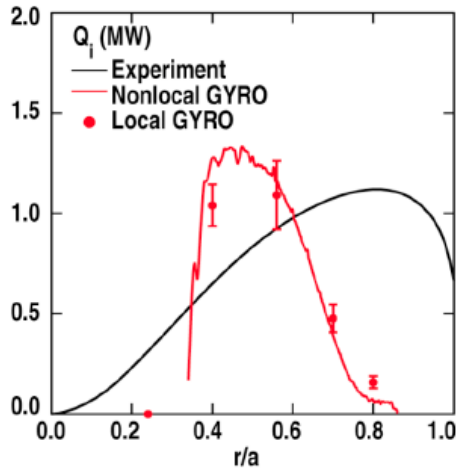
Figura 6.4: Ion heat flux underprediction in GYRO simulation of DIII-D [credit: C. Holland]

An posterior analyses (T. Görler *et al.*, 2014) realized with the use of GENE re-established the underprediction in the scenario above described. In Görler's work, an attempt to correct the past outcomes, and match the gyrokinetic predictions with the results from the diagnostic system is done.

Following the physical description of some input parameters of the discharge, the experimental set up can be reproduced as input of the GENE code. The main parameters of concern are the radial particle and heat transfer rate.

An analysis of the different microinstabilities taking place in the problem is done with the help of linear scans, an useful feature present in the GENE code. It allows us to run simultaneous simulations with different specific parameters, and therefore, give us the possibility to measure the impact of factors playing relevant roles in parameters of interest.

It is identified that, for a value of toroidal mode number in the rage between 10 - 100, substantially ITG driven modes are seen in the linear simulations. In figure 6.5, it can be seen by the positive upturn in the sign of the frequency of the instability. The black lines represent the two radial position of interest. The underprediction took place in the outer layer, and the horizontal grid represent the zero for the frequency w.

Other instabilities such as ETG and TEM do not contribute substantially to the ion heat transport in this case, and were not taken in account in the present analysis.

Since the issue with the past simulation may be related to the critical value of the mode exci-
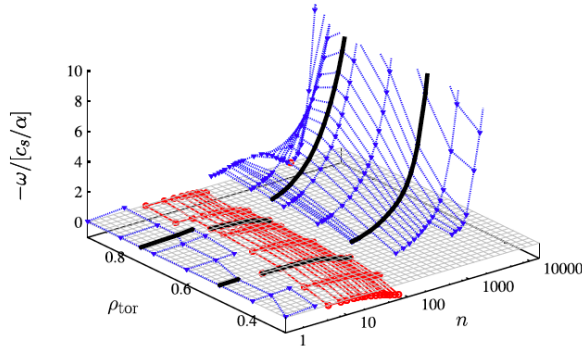
Figura 6.5: Negative frequency versus toroidal mode number and radial position [credit: T. Görler]

tation due to uncertainties in the input, a series of scans within the 30% of experimental errors is done in some of these parameters.

It is found that inside the errors margins, no significant impact is caused due to variation in the parameters. The collisional effect have reasonable impact on the TEMs, but negligible on the ITG mode. Ion temperature gradients are identified as the most impacting effect, when considered in the toroidal region of interest.

Outer-core nonlinear simulations with GENE gives us a smaller underprediction than the one obtained with the GYRO code. In here, a factor of 2 in the transport is found, rather than a factor of almost 7 as in the previous case.
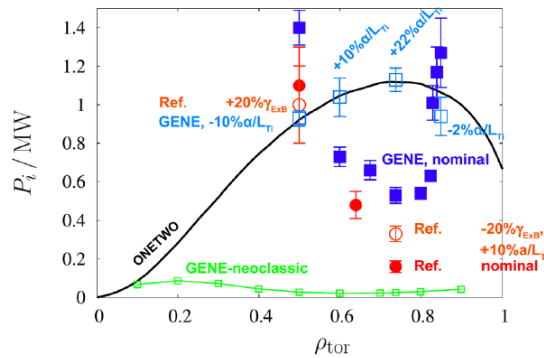

Figura 6.6: Ion heat transfer of GENE simulations the ONETWO experimental values [credit: T. Görler]

As we can observe in figure 6.6, the GENE simulations with the nominal values of parameters, in blue, underpredicts the ONETWO reconstruction only by a factor of approximately 2 in the region of interest. The simulations are done, also, considering a 20% margin within the range of accuracy. Light blue is the GENE case with variations in the temperature gradient parameter α/L_{Ti}, the logarithmic temperature gradient, and it seems to almost perfectly reproduce the experimental curve. The red and orange points represents the nominal and varied values for the

66

previous simulation made by C. Holland *et al.* In the orange case, considerations on the $E \times B$ shear flow were taken into account, this shear must be also considered in the GENE case, since the shear flow and parallel flow shear have an important effect in turbulence. Neoclassical transport is also shown and interestingly it demonstrates the difference in levels between the different transports.

6.3 ELECTROMAGNETIC STABILIZATION

A well known effect thought to be associated with the reduction of ITG instability and of turbulent heat transport is the electromagnetic (EM) stabilization. The electromagnetic finite β stabilization happens when the ballooning parameter $\alpha \sim q^2 \sum_i \beta_i$ approaches the threshold of the ideal magnetohydrodynamic MHD ballooning mode.

A study (J. Citrin *et al.*, 2015) investigates the impact of finite β electromagnetic and shear stabilization at high-β scenario in JET discharges. The Joint European Torus (JET) is the world's largest operational tokamak, located at Oxfordshire, in United Kingdom.

By examining the stiffness reduction in both inner and outer core radii, a study of the impact of microturbulence stabilization is done with the assistance of GENE nonlinear simulation, and experimental heat fluxes are retrieved. Stiffness is, then, defined as:

> "The gradient of the gyroBohm normalized ion heat flux with respect to the driving normalized logarithmic ion temperature gradient R/L_{T_i}."

It is found that the inclusion of fast ions increases the suprathermal pressure gradients, increasing the EM stabilization effects. It is important to assess the presence of fast ions due to the relevance to ITER-like scenarios, where toroidal rotation will not be as prone as in present cases, and the presence of fusion born α particles will change the EM dynamics of the system.

The definition of the parameter β/β_{crit} is done in order to facilitate the analysis of the impact of the EM ion mode with relation to its kinetic β limit. From the β definition, we can see that an increase in ITG stabilization is expected around the β limit imposed in this case. We must take into consideration, thus, that suprathermal pressures can increase the pressure gradient ($\sim \beta$) and therefore enhance the stabilization mechanism.

With the support of a series of linear simulations carried out at $k_y = 0.2$, the most unstable KBM mode, it is possible to establish a transition from ITG mode to a KBM mode.

KBM modes are Magnetohydrodynamical instabilities that originates in the plasma when high electromagnetic activity takes place due to high β effects.
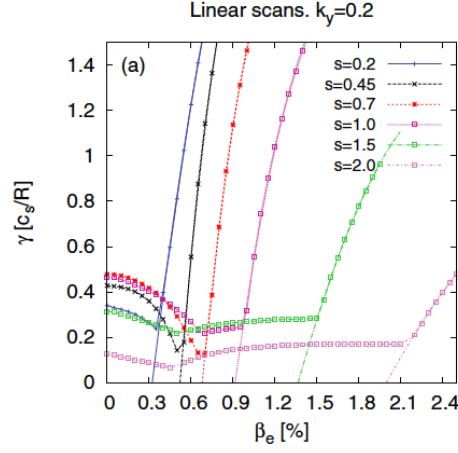

Figura 6.7: Linear growth rate and KBM threshold [credit: J. Citrin]

In figure 6.7 we can observe the sharp increase in the curve direction, characteristic of the ITG to KBM transition happening with the increase of β. The nominal value of the magnetic shear is $s = 0.7$, but the transition is observed for any value of s within the sensitivity scan. This study is important in order to assess the β_{crit} dependence with the low-s increased de-stiffening.

At lower s and with suprathermal pressure gradients, β_{crit} is found to be reduced, bringing the conclusion that enhanced ITG EM stabilization is expected at low s and high suprathermal pressure, generated by fast ions. For highly driven systems, in the studied case, $\beta_{KBM} < \beta_{NZT}$, considering β_{NZT} as the β of non-zonal transitions, an apparent reduction of zonal flow activity brought on by magnetic field perturbations affecting fluxes surfaces. This is an stimulating result, since the approach of $\beta \sim \beta_{KBM}$ has good impact on the ITG stabilization mechanism.

Inner core nonlinear simulations demonstrate a good agreement between numerical solutions and experimental values. The case is simulated with fast ions (30% reduced), without the fast ions, and with fast ions in an electrostatic scenario ($\beta = 0$).

In figures 6.8 and 6.9, we can observe the impact of the addition of fast ions on the ion and electron heat flux. The nonlinear EM stabilization is shown mostly as stiffness reduction, and it is crucial for the matching with the experimental flux values. Limits to the EM stabilization effects are found when the β/β_{crit} ratio is increased, and the KBM margin is passed. Decreases in β/β_{crit} are also related to the decrease in the stabilization mechanism in the curves with and without fast ions. Specifically in figure 6.9, we can observe that the impact in the electron heat flux is not as prone as in the ion case.
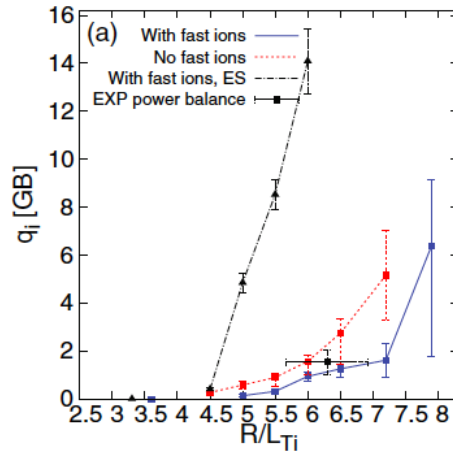
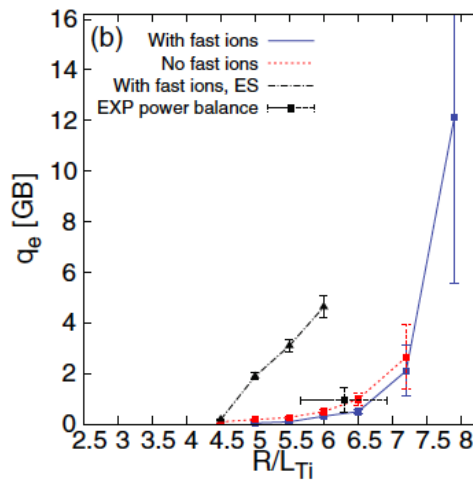Figura 6.8: Ion Heat Flux at inner radius [credit: J. Citrin]

Figura 6.9: Electron Heat Flux at inner radius [credit: J. Citrin]

This results are extremely encouraging not only as a support to the validation of the gyrokinetic theory, but also to the use of this theory as a predictor of high-β regime in ITER like scenarios, where low rotation and high suprathermal pressure gradients are more likely to take place, just as the case here analyzed.

6.4 SUMMARY

In this chapter, we have seen how the use of numerical solutions in the framework of the gyrokinetic theory can help us to match simulations with experimental results, helping us to understand underlying mechanisms taking place in specific underpredicted scenarios, and allowing us to extrapolate our assumptions to ITER like scenarios, since the control over a set of input parameters grant us the possibility to study sensitivity scans and, within uncertainties and the error bars, predict possible results to case not yet fully experimentally investigated.

The use of such tools is of extreme importance, since experiments take a long period of time to be done, and in most cases costs enormous amount of money, not to mention the bureaucratic factor in experiments of global scale such as ITER. What is more, these findings gives us adequate arguments to validate the use of GENE and the gyrokinetic approach to the representation of real tokamak-like microturbulent phenomena.

In the course of this work, we have studied the physics of transport of particles and heat in toroidally confined plasmas. We have seen how the different confinement models have evolved at the same time that a more particular description of the magnetic geometry was developed. We have seen, then, how the problem of higher-than-expected flux levels could be solved with the support of the gyrokinetic theory of turbulent transport. The use of extensive computer simulations is of utter importance for the realization of such task, and the usage of a highly parallelized gyrokinetic numerical code was introduced and explained.

Below, a short overview of the main outcomes of this work is discussed. More comprehensive descriptions can be found at the ends of some of the respective chapters.

7.1 SUMMARY

Plasma Confinement

In this section, we explained the different confinement models for thermonuclear controlled plasmas, and an analytical development of the theoretical framework for toroidal confinement was given. A study of a first approach for the transport theory is shown, and the conservation of the main quantities was demonstrated.

Realistic models

After a review of the more general approach to the transport theory, the tokamak concept is introduced and realistic transport models are discussed in this groundwork. An extensive analysis of the theoretical framework allows us to derive the foundations of the neoclassical transport, and the concept of anomalous transport is introduced as a mean to categorize the higher-than-expected flux levels.

Anomalous Transport

In order to sane the higher-than-expected flux levels, turbulent theory is shown as a well suited foundation that explains a series of features present in real cases experiments. For this reason, the gyrokinetic approach is used as a tool to analytically assess the underlying turbulent mechanisms

present in tokamak-like geometries. Ballooning properties are shown, and three main types of microinstabilities are discussed.

Numerical Approach

In order to validate the gyrokinetic theory, a numerical approach is introduce in the scope of high performance computing. Due to the nature of the phenomena in question, the use of single core computer to simulate relevant cases is not satisfactory. For that reason, an introduction to High Performance Computing is given, and the particularities of the field are briefly explained. The chapter follows with the introduction to the Gyrokinetic Electromagnetic Numerical Experiment, a highly parallelized code used to compute microturbulence analysis in thermonuclear toroidally confined plasmas.

Examples

In this section, we observed how the GENE code helps us in the validation of the gyrokinetic theory by answering open questions in the literature, and clarifying mechanisms not fully understood from experimental results. Here, an extended analysis of three paper is done, and an impartial analysis of the impact of the code on the description of experimental phenomena is discussed. It is found that most of GENE results are in good agreement with the experimental events, and that the analysis explains with good assertion the problems involving turbulent transport, mostly associated with the stabilization of the ITG microinstability.

7.2 OUTLOOK

The use of extensive computer resources have helped tremendously the Fusion community, but much more needs to be done. Here, it is shown the analysis of problems around the ion gyro-radii scale, but the coupling with problems in the MHD frequency scale and free-mean-path scale is needed. In order to do so, a series of approximation in both theories must be done. An optimization of numerical solutions must be accomplished, not only in the software but also in the hardware point of view, since the use of extensive computing time will be always part of the quest for sustainable fusion energy.

A more complete theoretical framework for the study of gyrokinetic theory could be also extended, mainly with respect to the development of more accurate collision operators and operators related to wave-particle interaction. A broader phenomenological study would be also required, in order to expand the understanding of the anomalous transport through another optics, *e.g.* non-

local transport.

To conclude, with great struggle from different levels, theoretical and computational plasma physics are capable of contributing to the design and, in the future, construction of a working fusion power station, helping us to content the energy necessities of the near future.

Bibliography

Albergante, M., Graves, J. P., Fasoli, A., Jenko F., and Dannert, T. Anomalous transport of energetic particles in iter relevant scenarios. Physics of Plasmas, 16(11):112301, 2009.

Bittencourt, J.A. Fundamentals of Plasma Physics. Springer New York, 2013.

Boozer, Allen H. Physics of magnetically confined plasmas. Rev. Mod. Phys., 76:1071–1141, Jan 2005.

Bovet, A. An Introduction to Non-diffusive Transport Models. ArXiv e-prints, August 2015.

Braginskii, S. I. Transport Processes in a Plasma. Reviews of Plasma Physics, 1:205, 1965.

Carmody, D., Pueschel, M. J., and Terry, P. W. Gyrokinetic studies of microinstabilities in the reversed field pinch. Physics of Plasmas, 20(5):052110, 2013.

Citrin, J., Jenko, F., Mantica, P., Told, D., Bourdelle. C., Garcia, J., Haverkort, J.W., Hogeweij, G.M.D., Johnson, Thomas., and Pueschel, M,J. Nonlinear stabilization of tokamak microturbulence by fast ions. Physical review letters, 111(15):155001, 2013.

Conner, J W., and Wilson, H. R. Survey of theories of anomalous transport. Plasma Physics and Controlled Fusion, 36(5):719, 1994. 79 J.W. Connor. Magnetic confinement theory summary. Nuclear Fusion, 45(10):S1, 2005.

Coronado, M., and Wobig, H. On the definition of pfirsch–schluter and bootstrap currents in toroidal systems. Physics of Fluids B: Plasma Physics, 4(5):1294–1300, 1992.

Diamond, P. H., Itoh, S-I, Itoh, K, and Hahm, T. S. Zonal flows in plasma—a review. Plasma Physics and Controlled Fusion, 47(5):R35, 2005.

Dimits, A. M., Bateman, G., Beer, M. A., Cohen, B. I., Dorland, W., Hammett, G. W., Kim, C., Kinsey, J. E., Kotschenreuther, M., Kritz, A. H., Lao, L. L., Mandrekas, J., Nevins, W. M., Parker, S. E., A. Redd, J., Shumaker, D. E., Sydora, R., and Weiland, J.. Comparisons and physics basis of tokamak transport models and turbulence simulations. Physics of Plasmas, 7(3):969–983,

2000.

Dnestrovskij, Y.N., Self-Organization of Hot Plasmas: The Canonical Profile Transport Model. Springer International Publishing, 2014. 74

Dorland, W., Jenko, F., Kotschenreuther, M., and Rogers, B. N. Electron temperature gradient turbulence. Phys. Rev. Lett., 85:5579–5582, Dec 2000.

ITER Physics Basis Editors, ITER Physics Expert Group Chairs, Co-Chairs, ITER Joint Central Team, and Physics Integration Unit. Chapter1: Overview and summary. Nuclear Fusion, 39(12):2137, 1999.

Eriksson, L-G., Hellsten, T., Nave, M. F. F., Brzozowski, J., Holmström, K., Johnson, T., Ongena, J., Zastrow, K-D., and JET-EFDA Contributors. Toroidal rotation in rf heated jet plasmas. Plasma Physics and Controlled Fusion, 51(4):044008, 2009.

Freidberg, J.P. Plasma Physics and Fusion Energy. Cambridge University Press, 2008.

Grad, H. and Rubin, H. Hydromagnetic Equilibria and Force-free Fields. U.S. Government Printing Office, 1958.

Gropp, W., Lusk, E., and Skjellum, A. Using MPI: Portable Parallel Programming with the Message-passing Interface. Number v. 1 in Scientific and engineering computation. MIT Press, 1999.

Görler, T., White, A. E., Told, D., Jenko, F., Holland, C., and Rhodes, T. L. A flux-matched gyrokinetic analysis of diii-d l-mode turbulence. Physics of Plasmas, 21(12):122307, 2014.

Hagan, W. K. and Frieman, E. A. Nonlinear gyrokinetic theory, the direct interaction approximation, and anomalous thermal transport in tokamaks. The Physics of Fluids, 29(11):3635–3638, 1986.

Hasegawa, Akira and Mima, Kunioki. Stationary spectrum of strong turbulence in magnetized nonuniform plasma. Phys. Rev. Lett., 39:205–208, Jul 1977.

Hastie, R. J., and Taylor, J. B. Stability theory of general plasma equilibria. ii. multipoles. Plasma Physics, 13(4):265, 1971.

Havlin, S., and ben-Avraham, D. Diffusion and Reactions in Fractals and Disordered Systems (Cambridge University Press, 2000)

Helander, Per. Theory of plasma confinement in non-axisymmetric magnetic fields. Reports on Progress in Physics, 77(8):087001, 2014.

Hirose, A. On finite stabilization of the toroidal ion temperature gradient mode. Physics of Plasmas, 7(2):433–436, 2000.

Holland, C., Candy, J., Waltz, R. E., White, A. E., McKee, G. R., Shafer, M. W., Schmitz, L., and Tynan, G. R. Validating simulations of core tokamak turbulence: current status and future directions. Journal of Physics: Conference Series, 125(1):012043, 2008.

Holland, C., Schmitz, L., Rhodes,, T. L., Peebles, W. A., Hillesheim, J. C., Wang, G., Zeng, L., Doyle, E. J., Smith, S. P., Prater, R., Burrell, K. H., Candy, J., Waltz, R. E., Kinsey, J. E., Staebler, G. M., DeBoo, J. C., Petty, C. C., McKee, G. R., Yan, Z., and White, A. E. Advances in validating gyrokinetic turbulence models against l- and h-mode plasmas. Physics of Plasmas, 18(5):056113, 2011.

Itoh, K., Toda, S., Fujisawa, A., Itoh, S.-I., Yagi, Fukuyama, M. A., Diamond, P. H., and Ida, K. Physics of internal transport barrier of toroidal helical plasmas. Physics of Plasmas, 14(2):020702, 2007.

Jenko, F., Dorland, W., Kotschenreuther, M., and Rogers, B. N. Electron temperature gradient driven turbulence. Physics of Plasmas, 7(5):1904–1910, 2000.

kamakshamma V., Sravanthi, G., Grace, B. A review of high performance computing. 2014.

Lyman Spitzer Jr. The stellarator concept. The Physics of Fluids, 1(4):253–264, 1958. 75

Lawson, J. D. Some criteria for a power producing thermonuclear reactor. Proceedings of the Physical Society. Section B, 70(1):6, 1957.

Mavridis, M., Isliker, H., Vlahos, L., Görler, T., Jenko, F., and Told, D. A study of self organized criticality in ion temperature gradient mode driven gyrokinetic turbulence. Physics of Plasmas, 21(10):102312, 2014.

McMillan, B. F., Jolliet, S., Tran, T. M., Villard, L., Bottino, A., and Angelino, P. Avalanche-like bursts in global gyrokinetic simulations. Physics of Plasmas, 16(2):022310, 2009.

Morozov, A.I. Introduction to Plasma Dynamics. CRC Press, 2012.

University of Wisconsin-Madison. Dept. of Nuclear Engineering, Engineering Physics, University of Wisconsin. Center for Plasma Theory, and Computation. University of Wisconsin Center for Plasma Theory and Computation report. University of Wisconsin Center for Plasma Theory and Computation Report. Nuclear Engineering and Engineering Physics Dept., 2002.

Pueschel, M. J., Terry, P. W., Jenko, F., Hatch, D. R., Nevins, W. M., Görler, T., and Told, D. Extreme heat fluxes in gyrokinetic simulations: A new critical . Phys. Rev. Lett., 110:155005, Apr 2013.

Pusztai, Istvan. Turbulent and Neoclassical transport in tokamak plasmas. PhD Thesis. Chalmers University of Technology, 2011.

Rogers, B. N., Kobayashi, S., Ricci P., Dorland W., Drake J., and Tatsuno, T. Physics of Plasmas (1994-present) 14, 092110 (2007)

Shafranov, V. D. Equilibrium of a toroidal plasma in a magnetic field. Journal of Nuclear Energy. Part C, Plasma Physics, Accelerators, Thermonuclear Research, 5(4):251, 1963.

Singh, R., Kaw, P.K., and Weiland, J. Non-linear features of the electron temperature gradient mode and electron thermal transport in tokamaks. Nuclear Fusion, 41(9):1219, 2001.

Shultis, J.K. & Faw, R.E. (2002). Fundamentals of nuclear science and engineering. CRC Press.

Wagner F., Fussmann, G., Grave, T., Keilhacker, M., Kornherr, M., Lackner, K., McCormick, K., Muller, E. R., Stabler, A., Becker, G., Bernhardi, K., Ditte, U., Eberhagen, A., Gehre, O., Gernhardt, J., Gierke, G. v., Glock, E., Gruber, O., Haas, G., Hesse, M., Janeschitz, G., Karger, F., Kissel, S., Kluber, O., Lisitano, G., Mayer, H. M., Meisel, D., Mertens, V., Murmann, H., Poschenrieder, W., Rapp, H., Röhr, H., Ryter, F., Schneider, F., Siller, G., Smeulders, P., Söldner, F., Speth, E., Steuer, K. H., Szymanski, Z., and Vollmer, O. Development of an edge transport barrier at the h-mode transition of asdex. Phys. Rev. Lett., 53:1453–1456, Oct 1984.

Weiland, J. and Hirose, A. Electromagnetic and kinetic effects on the ion temperature gradient mode. Nuclear Fusion, 32(1):151, 1992.

Wootton, A. J., Carreras, B. A., Matsumoto, H., McGuire, K., Peebles, W. A., Ritz, Ch. P., Terry, P. W., and Zweben, S. J. Fluctuations and anomalous transport in tokamaks. Physics of Fluids B: Plasma Physics, 2(12):2879–2903, 1990.